The local nature of the plasma response to cold pulses with electron and ion heating at ASDEX Upgrade

C. Angioni[1], E. Fable[1], F. Ryter[1], P. Rodriguez-Fernandez[2], T. Pütterich[1], and the ASDEX Upgrade Team

[1]Max–Planck–Institut für Plasmaphysik, Boltzmannstrasse 2, D–85748 Garching, Germany

[2] MIT Plasma Science and Fusion Center, Cambridge, Massachusetts 02139, USA

E-mail: clemente.angioni@ipp.mpg.de

Abstract. In low density Ohmic heated tokamak plasmas a fast increase of the central electron temperature is regularly observed in response to a drop at the edge produced by the cold pulse of an impurity ablation. This observation has challenged the physical understanding and the theory–based local transport modelling for several decades. Recent experimental results in C-Mod and related modelling [P. Rodriguez-Fernandez et al 2018 Phys. Rev. Lett. **120**, 075001] have for the first time provided an explanation to this phenomenology, which results from the stabilization of trapped electron mode turbulence caused by the sudden flattening of the electron density profile as a consequence of the impurity ablation. Starting from this breakthrough result, recent cold pulse experiments in ASDEX Upgrade produced by laser ablation of carbon in deuterium plasmas demonstrate that the fast increase of the central electron temperature is only observed in the presence of dominant electron heating, whereas no fast increase is observed in dominantly ion heated plasmas, even though at the same low density. The measured fast flattening of the density profile is shown to be large enough to produce a strong stabilization of the trapped electron mode turbulence in case where the electron temperature largely exceeds the ion temperature, allowing the fast increase of the central electron temperature, consistent with the C-Mod modelling results. In contrast, it produces a destabilization of the electron temperature gradient modes when electron and ion temperatures are closer, preventing the increase of the central electron temperature. Finally, modelling which also includes the dynamical evolution of the density profile with a local theory–based transport model, shows that the impurity penetration transiently modifies the local turbulence causing a fast penetration of the particles, which explains the observation of a very fast flattening of the electron density profile. By this, the complex density and temperature behaviours in response to a cold pulse are demonstrated to be fully explained by multi–channel interactions within a local model.

1. Introduction

In tokamaks, the plasma response to cold pulses has been subject of a large number of investigations, in particular due to the puzzling observation that, under certain plasma conditions, the electron temperature increases in the center very quickly, just after it starts to drop at the edge [1–12]. This behaviour, which leads to a very fast increase of the electron temperature gradient over a large portion of the plasma cross section in response to the reduction of the temperature at the edge, has been often referred to as "non–local" [13, 14], as it was argued that these observations cannot be explained by conventional local diffusive transport. In particular, a rapid increase of the central electron temperature in response to a peripheral drop is observed in low confinement (L–) mode plasmas with Ohmic heating (OH) at low densities, usually corresponding to conditions where the linear Ohmic confinement (LOC) occurs, whereas a conventional diffusive behaviour, with a reduction of the central electron temperature slowly following the edge drop is observed at higher densities, like in the saturated Ohmic confinement (SOC) regime. An even larger central increase of the electron temperature at low density is observed in the presence of additional auxiliary central electron heating [15]. While these observations have been regularly reported to be inconsistent with the assumptions of local transport, an early modelling attempt [16] with theory–based transport models opened the possibility that they could still be explained by local transport models which include critical temperature gradients and which involve strong dependences on local parameters, as it is predicted for usual core micro–instabilities like ion and electron temperature gradient (ITG and ETG) modes, as well as trapped electron modes (TEM). An important property of turbulent transport in general is that the behaviour of one transport channel is strongly affected by plasma parameters which are determined by other transport channels. These theoretically predicted, and often experimentally observed, multi–channel interactions suggest that the correct approach to the study of the dynamical response of the electron temperature to peripheral cold pulses cannot be properly described by a model which is limited to the electron heat transport channel only and it is exclusively determined by the electron temperature evolution.

Recent experiments in C-Mod and related modelling [17, 18] have finally clarified that, at least in tokamaks, this supposed "non–local" behaviour observed at low density can be indeed reproduced by a local theory–based transport model like TGLF [19], with its most recent saturation rule TGLF–SAT1 [20, 21], when the impact of the time evolution of the electron density profile evolution is taken into account in the prediction of the time evolution of the electron temperature. In the simulations, a fast reduction of the electron heat transport and a sudden increase of the central electron temperature of comparable magnitude to that experimentally measured is caused by the sudden flattening of the plasma electron density profile which follows the peripheral laser ablation of the impurity. This result is certainly a major breakthrough in the understanding of these observations, and gives a solution to one of the most long–standing open problems in the transport of tokamak plasmas. Moreover, this result confirms that the local transport model approach, which is regularly applied in the

prediction of future reactor plasmas, can also explain the plasma dynamics of these challenging experimental results.

At the same time, this landmark obtained from the modelling of C-Mod plasmas opens the way to related new applications in the theory–based transport modelling of the dynamical plasma response to external perturbations, and allows us to identify some new questions for the next steps in the research in this topic.

A current study on DIII-D [22] confirms the results obtained on C-Mod. It demonstrates that in low density OH plasmas the rapid density flattening produced by the laser ablation and measured by reflectometry is indeed compatible with the electron heat transport reduction which is required by TGLF to obtain the central temperature increase which is experimentally observed. This study also delivers a correct theoretical prediction of the density at which a change in the sign of the central electron temperature perturbation is experimentally observed.

In the present work, we consider some of the remaining open questions by means of a combination of new experiments in ASDEX Upgrade (AUG) and related theory–based modelling, with particular emphasis on the role of auxiliary electron and ion heating and the simultaneous modelling of the temperature and density dynamical behaviours.

In particular,

- Is the physical explanation proposed in Ref. [17, 18] for C-Mod consistent with observations in ASDEX Upgrade?
- Is the observed density flattening in AUG large enough to produce a significant stabilization of turbulence under appropriate conditions and when does this take place?
- How is the plasma response to cold pulses in OH plasmas related to the response in the presence of additional electron and ion auxiliary heating, and what is the role of the density profile evolution in these heating conditions?
- Finally, is the fast flattening of the electron density profile consistent with the dynamical predictions of a local transport model, like TGLF, or does the fast evolution of the density profile still require a non–local assumption for its description ?

To answer these questions, in this work we have carried out a set of cold pulse experiments in AUG in OH and with auxiliary ion and electron heating and performed related predictive modelling with the transport code ASTRA [23, 24] coupled to the local quasi–linear transport model TGLF-SAT1 [19–21] and the impurity transport code STRAHL [25–29].

From the experimental standpoint, differently from previous works, where the plasma response to cold pulses was mainly investigated as a function of the plasma density, in the present work we have investigated the plasma response to cold pulses as a consequence of a variation of the ion to electron heat flux ratio, also at the same low density. To this end, in addition to OH plasmas, plasmas with central electron cyclotron resonance heating (ECRH) and neutral beam injection (NBI) heating have been obtained, and a low NBI voltage has been applied in order to increase the ion

heating fraction produced by the NBI. Four different experimental scenarios have been investigated, low density and intermediate density plasmas with Ohmic (OH) heating, and low density plasmas with central ECRH and with central NBI. Of course, the application of NBI in comparison to ECRH not only implies a variation of the electron and ion heat fluxes, but also implies the addition of a particle source and of a torque, with impact on the density and rotation profiles. These additional unavoidable modifications of the plasma conditions are assumed not to be the main elements which determine whether an increase of the central electron temperature is observed or not in response to a peripheral cold pulse. This assumption is supported by the observation that a transition in the plasma response to cold pulses is regularly observed with increasing density in OH plasmas, thereby in the absence of an external particle source and an external torque.

The experimental results are then used as terms of comparison for the transport modelling with the code ASTRA and the transport model TGLF-SAT1. Two different modelling strategies have been followed. In the first strategy, only the time evolution of the electron and ion temperature profiles are modelled, while the time evolution of the density profile is taken from the experimental measurements. With this simulation approach we investigate whether the experimentally measured density flattening is large and fast enough to induce electron temperature perturbations which match those which are observed, and we test whether the assumption of a constant density profile during the cold pulse (that is, kept fixed to the last measurement before the cold pulse) prevents to obtain the observed behaviour of the electron temperature profile in the simulations. This first modelling strategy thereby aims at confirming the modelling results and the physical explanation obtained in C-Mod on the AUG data. The second modelling strategy includes also the simulation of the density profiles. To this end, we include also the dynamical modelling of the carbon impurity injected by laser ablation, by means of the code STRAHL, and we simulate the consequent impact of this on the time evolution of both the density and temperature profiles of the deuterium and electron species.

The remainder of this paper is organized as follows. In Section 2 the experiments are presented and the different responses of the electron temperature to the peripheral cold pulses in the different experimental scenarios are described. Correlations among the central electron temperature variations due to the cold pulses and the electron to ion heat fluxes are pointed out. In Section 3, the results of the transport modelling in which only the electron and ion temperature profiles are simulated are presented. The simulation results are compared with the observations in the four experimental scenarios. Finally in Section 4, the results of the transport simulations in which also the time evolution of the density profiles are included are presented. Here the focus is on the experimental case with central ECRH at low density, in which the highest increase of central electron temperature is observed in response to the cold pulse.

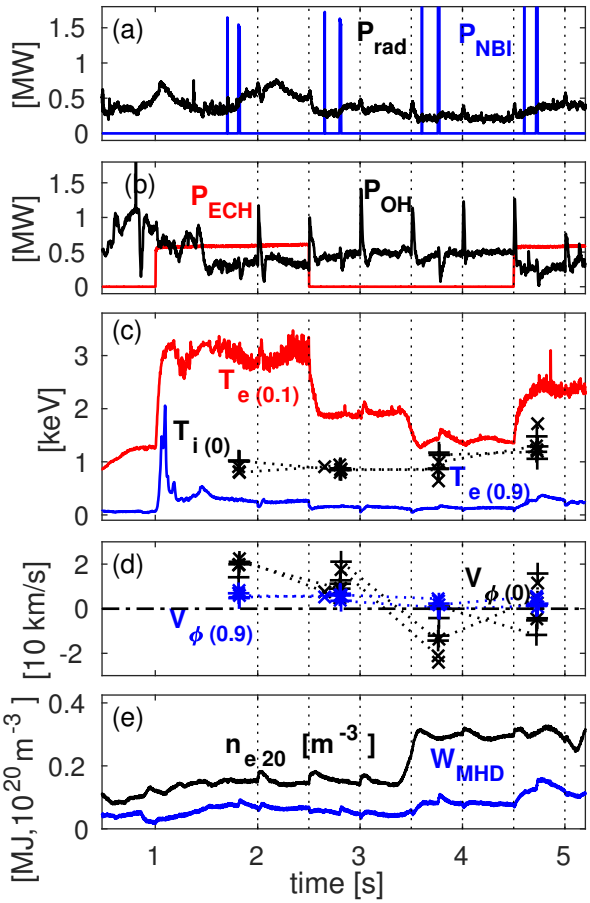

Figure 1. Time traces of selected quantities of the AUG discharge ♯34525 with OH and ECRH phases, showing NBI and radiated power (a), ECRH and OH power (b), central and peripheral electron temperature and central ion (boron) temperature in logarithmic scale (c), central and peripheral boron toroidal rotation (d), line averaged density and total stored energy (e). Vertical dotted lines identify the time slices at which laser ablations of carbon have been performed, the values in brackets of the radial positions for the electron and ion temperatures and the boron toroidal rotation refer to ρ_ϕ.

2. Experimental results

The experimental results that are reported here have been obtained in a set of plasma discharges in the ASDEX Upgrade tokamak. The goal of these experiments is to investigate the plasma response to cold pulses by changing the electron to ion heat flux ratio keeping fixed the density. Thereby, the goal of these experiments can be considered somewhat complementary to the most common goal of the investigations which were performed previously, which were more regularly dedicated to the change in the plasma response to cold pulses with increasing density. All of the plasmas have a current of 800 kA, a magnetic field of 2.5 T, and a safety factor at the 95% of the toroidal flux $q_{95} = 4.8$. Plasma density has been varied during the discharges or from discharge to discharge, obtaining stationary phases at line averaged densities of 1.6 10^{19}

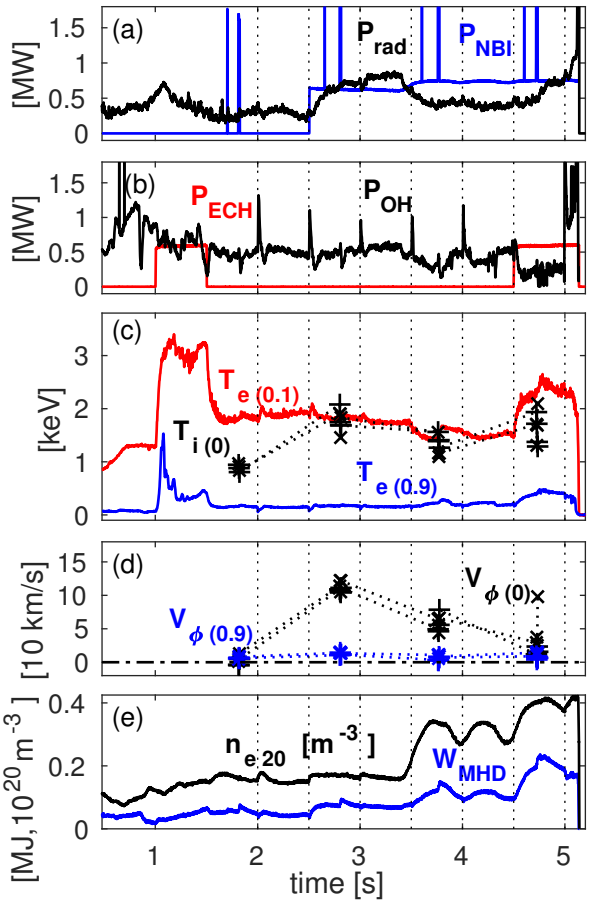

Figure 2. Time traces of selected quantities of the AUG discharge ♯34527 with OH and NBI heated phases, showing NBI and radiated power (a), ECRH and OH power (b), central and peripheral electron temperature and central ion (boron) temperature in logarithmic scale (c), central and peripheral boron toroidal rotation (d), line averaged density and total stored energy (e). Vertical dotted lines identify the time slices at which laser ablations of carbon have been performed, the values of the radial positions indicated in brackets for the electron and ion temperature and the toroidal rotation refer to ρ_ϕ.

m^{-3} and 3.0 10^{19} m^{-3}, which will be referred to as "low" and "intermediate" density phases. Multiple cold pulses have been produced during these stationary density phases by producing laser ablation of a carbon target. Time traces of a discharge featuring low and intermediate density phases with ECRH and OH phases are presented in Fig. 1, while Fig. 2 shows a corresponding discharge with NBI heating and OH phases. Vertical dotted lines identify the time slices at which a laser blow off has been performed. Blips of the NBI power, Fig. 1(a) and Fig. 2(a), have been included in order to obtain measurements of the boron temperature and toroidal rotation. Central ECRH reduces the OH power, which increases when the ECRH power is switched off Fig. 1(b) and Fig. 2(b). However, the deposition of the ECRH power is localized at $\rho_\phi \leq 0.1$ (where ρ_ϕ is the square root of the normalized toroidal flux), with a total absorbed power around 600 kW coming from one gyrotron, which is much more centrally localized than the

OH power density. As a consequence of this, the measured electron temperatures are significantly higher in the phases with central ECRH than in the OH phases at the same low density. The NBI heating is applied with reduced extraction voltage (35 kV in contrast to the maximum of 60 kV for the used AUG injector), delivering a total NBI power of about 750 kW only, comparable to the amount of ECRH power from one gyrotron, and increasing the fraction of central ion heating. Thanks to the different heating phases and densities, large variations of the electron to ion temperature ratio have been produced, Fig. 1(c) and Fig. 2(c). Good stationary phases with the same low line averaged density 1.6 10^{19} m^{-3} have been obtained with ECRH and NBI heating, as well as in OH, Fig. 1(e) and Fig. 2(e). A steady behaviour of the density has also been obtained at intermediate density 3.0 10^{19} m^{-3} in OH, whereas more difficult has been to keep the density steady at intermediate density values in the presence of auxiliary heating, due to a higher sensitivity of the plasma to the competing effects of the impurity ablation and the coupled reactions of the density evolution and the gas valves, connected to the stronger proximity to the transition to H–mode. In general, and as expected, all of the discharges have been terminated by total consumption of the OH flux, still during the current flat top phase. As an additional piece of information, also discharges with laser ablations of tungsten have been produced, but in this case no reversal of the electron temperature perturbation from negative at the edge to positive in the center has been observed, in any condition. STRAHL modelling has clarified that the cold pulses produced by tungsten are not edge localized, and significant radiation losses are produced also in the central region of the plasma, preventing the increase of the central electron temperature which in contrast can be observed when the cold pulse is localized at the edge, as it is the case with a lighter impurity like carbon.

Measurements of the electron temperature and electron density have been obtained by means of the AUG integrated data analysis (IDA) [30], particularly based on electron cyclotron emission radiometry [31], with a time resolution of 6.4 10^{-5}s, electron density interferometry [32], with a time resolution of 1.0 10^{-4}s, and lithium beam impact excitation spectroscopy [33], with a time resolution of 10^{-3}s. The high time resolution of all of these diagnostics allow the IDA to well resolve the time evolutions of the electron temperature and density during and after a cold pulse, with a time resolution of the IDA profiles of 10^{-3}s. The ion temperature and toroidal rotation profiles have been measured during short NBI blips of 13 ms [34,35] which have been performed during the stationary heating phases before the laser ablation shots. Thereby, ion temperature and toroidal rotation measurements are only providing reference profiles in the stationary phases, but cannot follow the time evolution during the cold pulses.

Five discharges of this type have been obtained, for a total of 22 successful laser ablations of carbon in the different stationary plasma phases. The time evolution of the electron temperature and of the density in 4 representative conditions, OH at low and intermediate density and with ECRH and NBI heating at low density, are shown in Figs. 3. We observe that in all the heating conditions, the impurity laser ablation produces a transient flattening of the density profile, with a sudden fast increase of the edge density which is followed only later by a weaker increase in the center. The

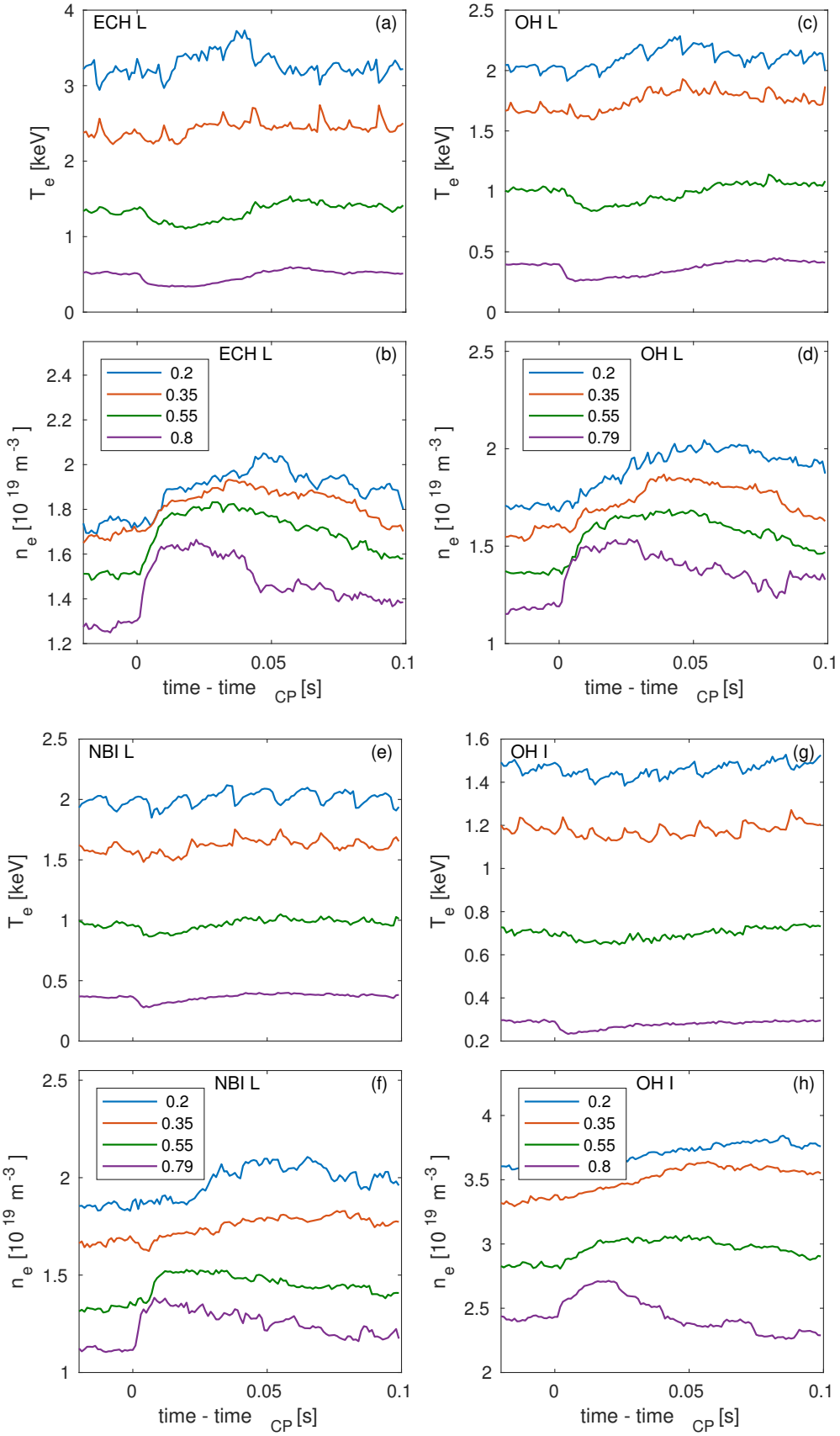

Figure 3. Time traces of the electron temperature (a,c,e,g) and the electron density (b,d,f,h) at four radial locations as indicated by the values of r/a in the legends as a function of time relative to the impurity blow off time, for heating phases at low density with ECRH ('ECH L') (a,b), low density OH ('OH L')(c,d), low density with NBI heating ('NBI L')(e,f) and intermediate density OH ('OH I')(g,h).

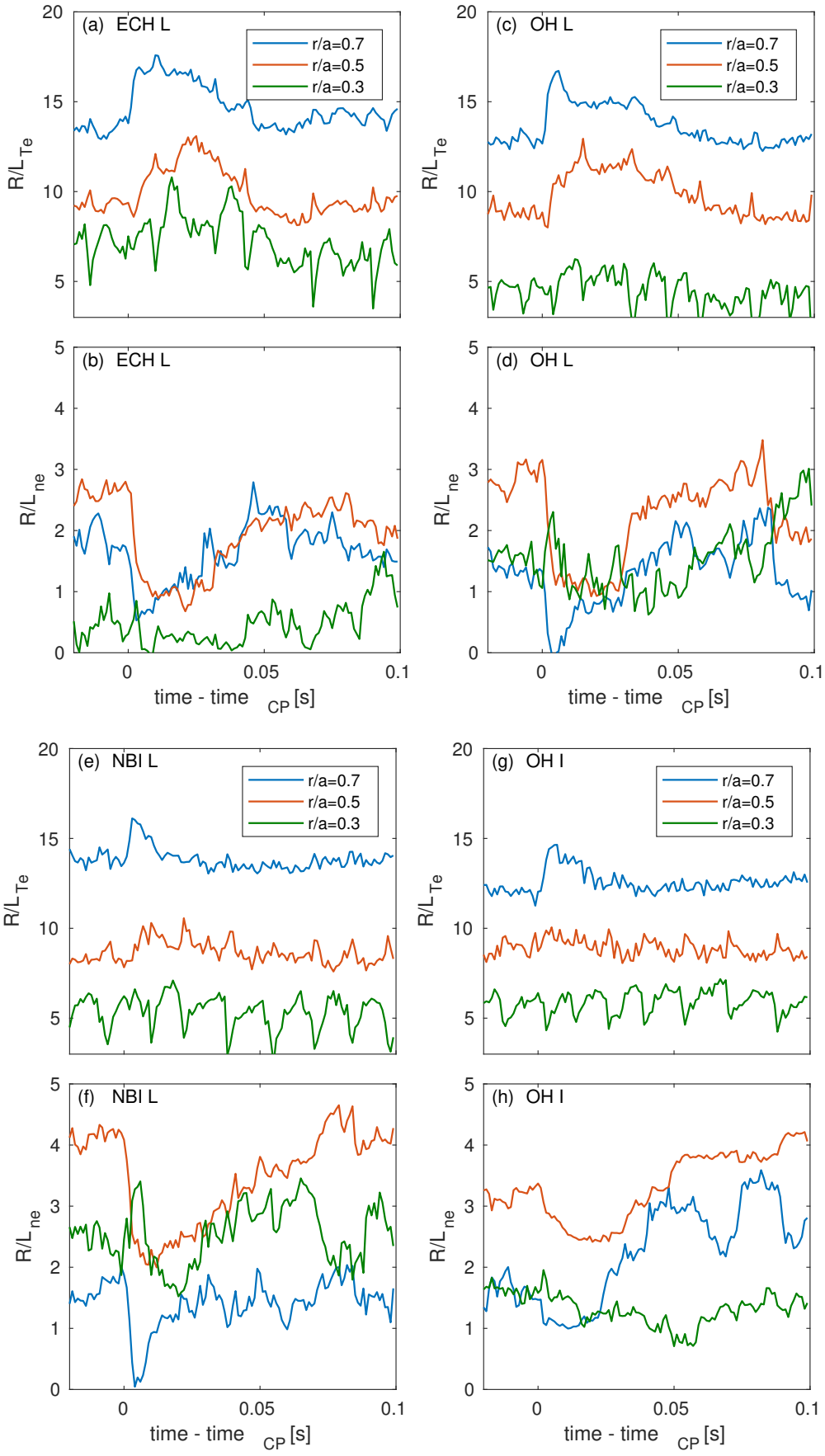

Figure 4. Time traces of the normalized electron temperature logarithmic gradient at (a,c,e,g) and the normalized electron density logarithmic gradient (b,d,f,h) at $r/a = 0.3$, $r/a = 0.5$ and $r/a = 0.7$ as a function of time relative to the impurity blow off time, for heating phases at low density with ECRH ('ECH L')(a,b), low density OH ('OH L')(c,d), low density with NBI heating ('NBI L')(e,f) and intermediate density OH ('OH I')(g,h).

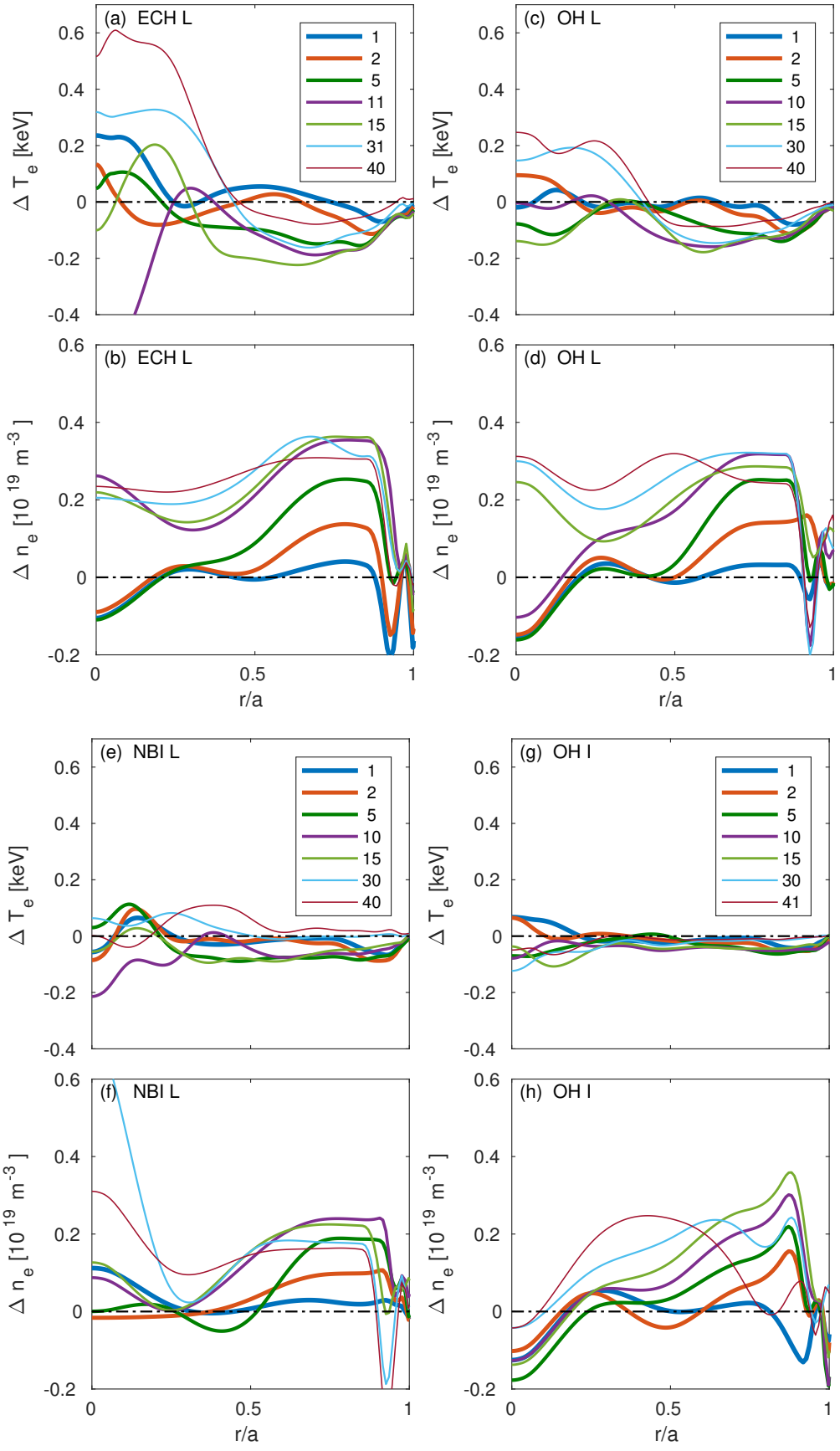

Figure 5. Time evolution of the electron temperature (a,c,e,g) and electron density (b,d,f,h) variations along the minor radius at different times after the cold pulse injection, as indicated by the values in the legend in ms, for heating phases at low density with ECRH ('ECH L')(a,b), low density OH ('OH L')(c,d), low density with NBI heating ('NBI L')(e,f) and intermediate density OH ('OH I')(g,h).

effect is however stronger at low density, and particularly in the electron heated cases, OH and central ECRH. The corresponding time evolution of the electron temperature is in contrast qualitatively different in the four cases. The electron heated cases, OH and central ECRH at low density, feature an increase of the electron temperature in the center in a phase in which the temperature at the edge is still lower than in the phase prior to the cold pulse, that is, the well-known inversion of the temperature perturbation from the edge to the core, often considered in the past as a signature of the presence of a non–local transport mechanism. Differently, the cases with NBI heating at low density and OH at intermediate density do not show any increase of the central electron temperature in the phase in which the edge temperature is reduced. These differences can be even better realized by looking at the time evolution of the logarithmic temperature and density gradients Fig. 4 at mid-radius. We observe that as a consequence of the cold pulse, the normalized logarithmic density gradient R/L_{ne} suddenly drops in all of the cases, although quantitatively more in the low density OH and ECRH cases, while the normalized logarithmic electron temperature gradient R/L_{Te} significantly increases only in those two cases. The drop in density gradient takes place in less than 5 ms, and is followed by the increase of the electron temperature gradient, which reaches its maximum later, after about 20 ms. We also observe that the sudden reduction of the electron density gradient is much faster than the relative change of the electron density, which also takes place on a longer time scale (10 to 20 ms). The time evolution of the profiles is shown in Fig. 5, where the differences between the electron temperature and density profiles from the corresponding profiles in the phase before the cold pulse are plotted for a set of time slices after the cold pulse (the corresponding time values, measured from the start of the laser ablation, are reported in milliseconds in the legends). The sudden increase of the density profile is evident in all of the cases, with a fast propagation inward which is completed in less than 10 milliseconds. The electron temperature has a very moderate evolution in the cases without dominant electron heating, whereas in the cases with dominant electron heating, it increases in the center with a delay of few milliseconds with respect to the density. We also notice the impact of a sawtooth crash after about 10 ms in the case with central ECRH. From the analysis of the time traces of the experimental profiles, it can be concluded that also in AUG experiments a significant flattening of the density profile is produced by the impurity laser ablation, which is consistent with the observations in C-Mod [17, 18] and DIII–D [22].

Power balance analyses by means of ASTRA interpretive runs have been performed for all of the heating phases. The profiles of the auxiliary heating power densities and of the corresponding integrated powers are presented in Fig. 6. For comparison, also the heating profiles from the NBI computed with full voltage (60 kV) are shown with dashed lines, highlighting the effect of having operated with reduced voltage (35 kV), which allows the electron to ion heat flux ratio produced by the NBI at $r/a = 0.5$ to be decreased from 0.36 to 0.165. The total heating power from the NBI approximatively matches that of the ECRH. In addition, also for direct comparison, the profiles of the radiated power due to the cold pulse as computed by STRAHL are shown in Fig. 6(a)

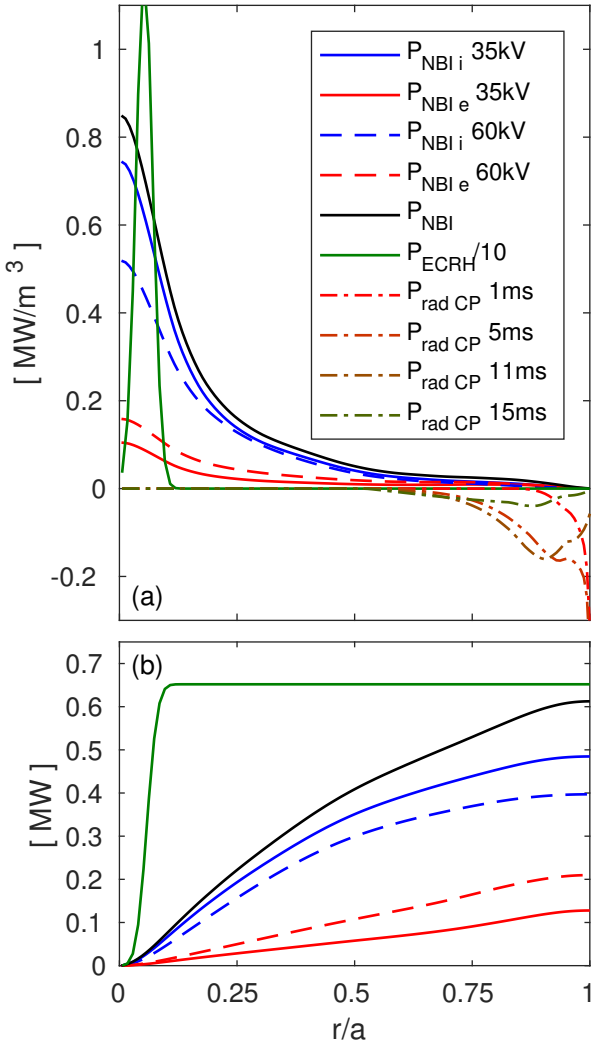

Figure 6. Profiles of the auxiliary heating power densities applied in these discharges with NBI and ECRH, and of the radiation profiles produced by the cold pulses as computed with STRAHL (a). Corresponding profiles of the volume integrated total powers of the auxiliary heating (b). For plotting purposes, in (a) the ECRH power density has been divided by 10. A comparison between the actually applied NBI reduced voltage of 35 kV with respect to the full voltage 60 kV (assuming the same total absorbed power) is presented in (a,b), demonstrating the increased ion heating fraction at 35 kV. The radiation profiles are presented at 1ms, 5ms, 11ms and 15ms after the start of the laser ablation, as reported in the legend.

with dash–dotted lines. The results of the power balance analysis are summarized in Fig. 7. The maximum electron temperature variations in keV around $r/a = 0.30$ during the phases after the cold pulses in which the edge temperature is reduced are shown in Fig. 7(a). The corresponding maximum temperature variations around $r/a = 0.85$ in the same time intervals are shown in Fig. 7(b). In both cases plots are made as a function of the electron to ion heat flux ratio Q_e/Q_i at mid–radius. The same central and peripheral temperature variations, but this time normalized to the corresponding local temperatures before the cold pulses, are plotted in Figs. 7(c,d) respectively, as a function

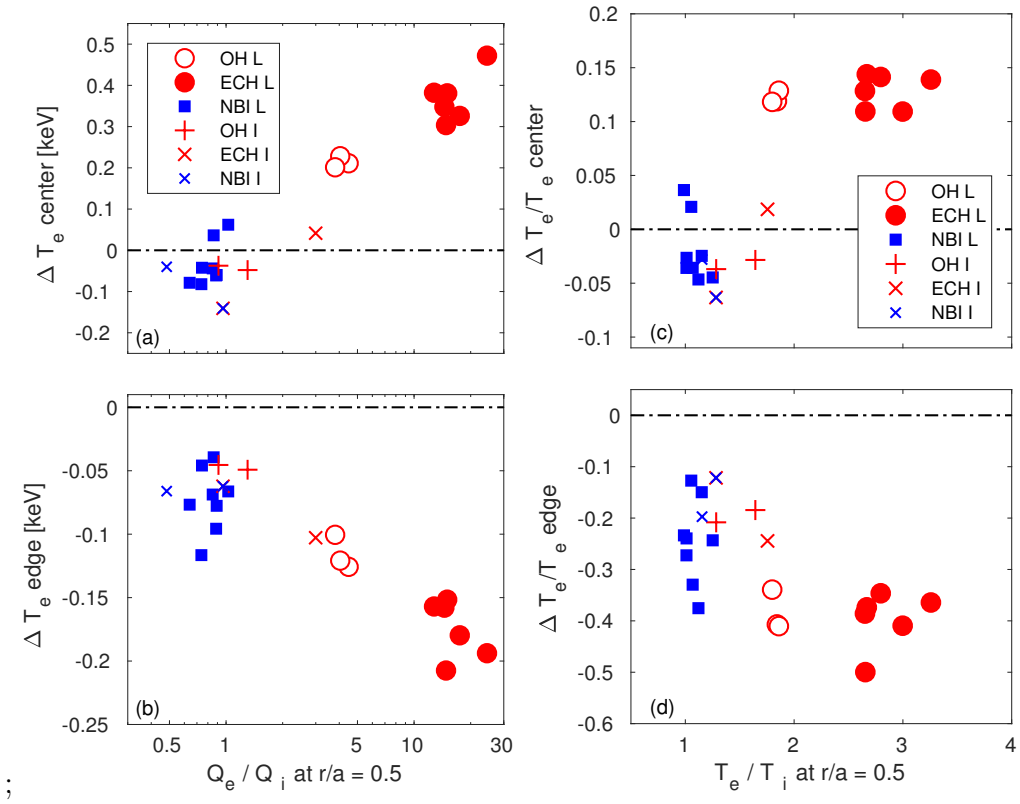

;

Figure 7. Absolute (a,b) and relative (c,d) variations of the electron temperature in the central ($r/a = 0.3$) (a,c) and peripheral ($r/a = 0.85$)(b,d) regions of the plasma as a function of the electron to ion heat flux ratio (a,b) and the electron to ion temperature ratio (c,d) at mid–radius ($r/a = 0.5$). Different symbols are used to identify different heating and density phases, as reported in the legend, OH at low (OH L) and intermediate (OH I) density, ECRH at low (ECH L) and intermediate (ECH I) density, NBI heating at low (NBI L) and intermediate (NBI I) density.

of the electron to ion electron temperature ratio at mid–radius. The plots identify clear relations between the variations of the central and the peripheral temperatures and the electron to ion heat flux ratio, which clearly disentangle the dependence on density with that on the heat flux ratio. The low density OH and ECRH phases feature the usual effect of increased peaking of the electron temperature profile in response to the cooling of the edge, whereas, in contrast, the NBI phases at the same low density do not exhibit any significant increase of the central electron temperature. The increase of central electron temperature, as well as the decrease of the edge temperature, are larger in the presence of ECRH heating than in OH conditions, although comparable when normalized to the corresponding temperatures before the cold pulse. A stronger absolute increase with central ECRH is consistent with the higher central electron heating power density in this case, for comparable reductions of the electron heat conductivity. In contrast, with NBI heating at the same low density, the central electron temperature has only a very limited variation after the cold pulse, with also a more limited drop at the edge, and a usually shorter phase during which the electron temperature at the edge is decreased (about 30 ms only compared to 50 ms in the electron heated cases).

Results similar to those with NBI heating at low density are obtained in all of the heating phases at intermediate density, featuring small and usually negative variation of the electron temperature in the center. We conclude that a clear central electron temperature increase in response to the edge cold pulse requires a large fraction of electron heating, whereas a low density is not a sufficient condition. All of the phases at intermediate density display very limited and in general negative variations of the electron temperature in the center. Analogous trends can be obtained plotting the temperature variations (this time relative to the temperature before the cold pulse, not to provide twice the same information) as a function of the electron to ion temperature ratio at mid-radius. A strong increase of the central electron temperature is obtained only in conditions in which the electron to ion temperature ratio is large. We also notice that the drop of the electron temperature at the edge as a consequence of the impurity injection is much larger in the case of plasmas with ECRH than in plasmas with NBI heating. This can be partly explained by the higher radiated power produced at higher electron temperature, as obtained with STRAHL, but also, and more importantly, by the stronger thermal coupling between electrons and ions which is obtained when the electron temperature is lower, and when the density is higher, leading to a reduced cooling effect on the electrons.

In conclusion, the analysis of the experimental results obtained in AUG shows that as a consequence of the impurity ablation the density is the first to react, producing a sudden flattening of the profile. The fast reduction of the density gradient is consistent with the analysis and modelling results obtained in C–Mod [17, 18] and DIII–D [22]. This density flattening is observed in all of the heating phases examined, but the amount of flattening (relative reduction of the logarithmic density gradient) is clearly stronger in the low density cases, as the relative particle perturbation produced by the impurity particle source is stronger. The electron temperature follows the electron density response, and exhibits an increase of the central electron temperature in the OH and ECRH phases at low density, that is in conditions in which the electron heating is dominant and the electron to ion temperature ratio is large. In contrast the electron temperature has a much smaller variation in conditions in which both the electron to ion heat flux and temperature ratios are close to 1, as it is obtained with NBI heating at low density, or at intermediate densities in all of the investigated heating phases, also in connection with the increased collisionality of the plasma.

3. Transport modelling with prescribed electron density

The experimental results presented in the previous section provide us with a significant amount of data against which the transport modelling can be performed in order to try to answer to the remaining questions that have been listed in the introduction. **We notice that theory–based quasi–linear transport models are more regularly applied to the prediction of stationary plasma conditions, over which a larger validation has been performed, but also to the dynamical evolution of the plasma discharges, e.g. [24, 36–38].** First we consider a modelling approach which

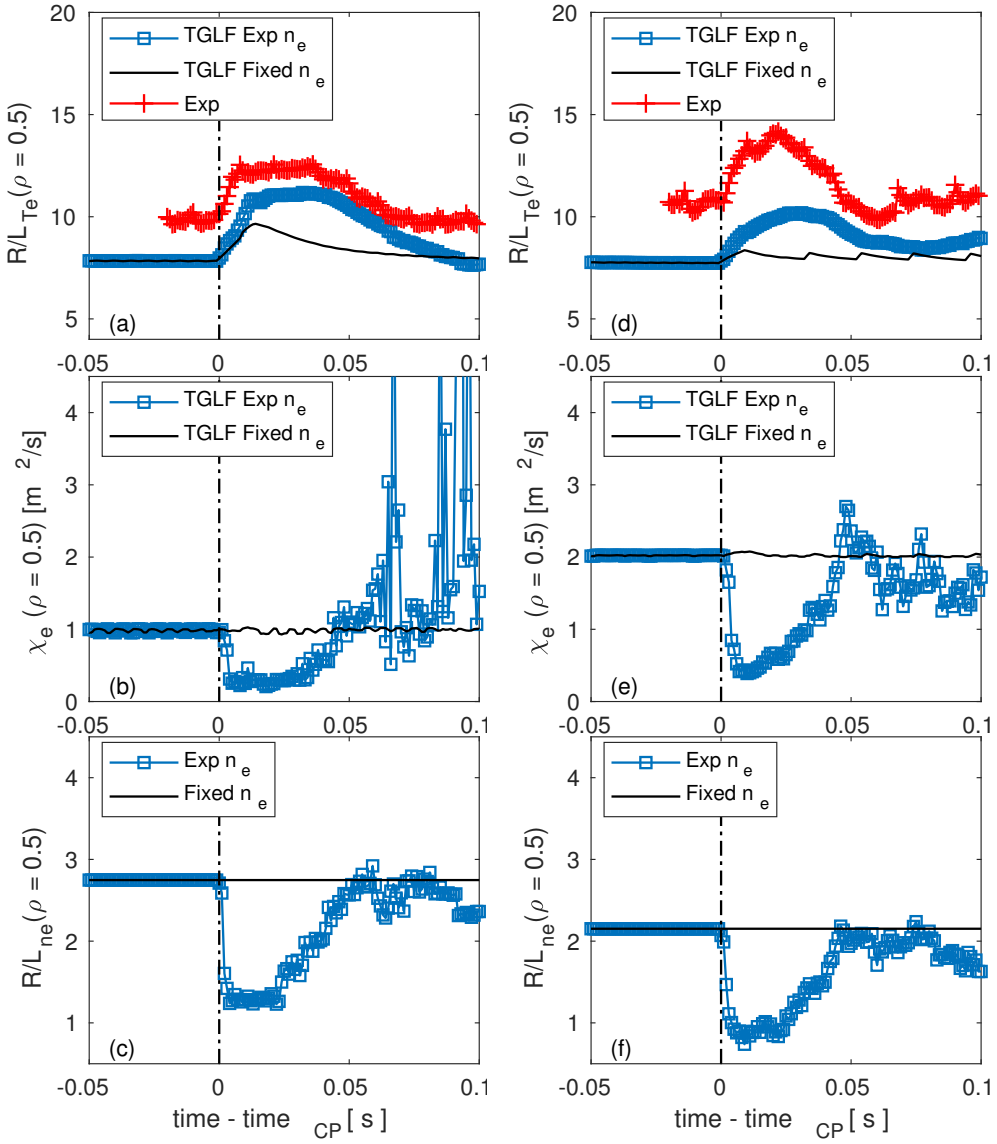

Figure 8. Time evolution of the normalized logarithmic electron temperature gradient at mid-radius ($\rho_\phi = 0.5$) obtained in the ASTRA / TGLF simulations (a,d) with prescribed density which follows the experimentally measured time evolution (squares) and which is kept fixed to the measured profile before the cold pulse (solid line), compared to the experimental measurements (crosses +). Corresponding evolution of the TGLF electron heat conductivity at the same radial location (b,e) and prescribed electron density logarithmic gradient in the ASTRA simulations (c,f). Two electron heated phases at low density are shown, a low density OH phase (a,b,c), a low density ECRH phase (d,e,f),

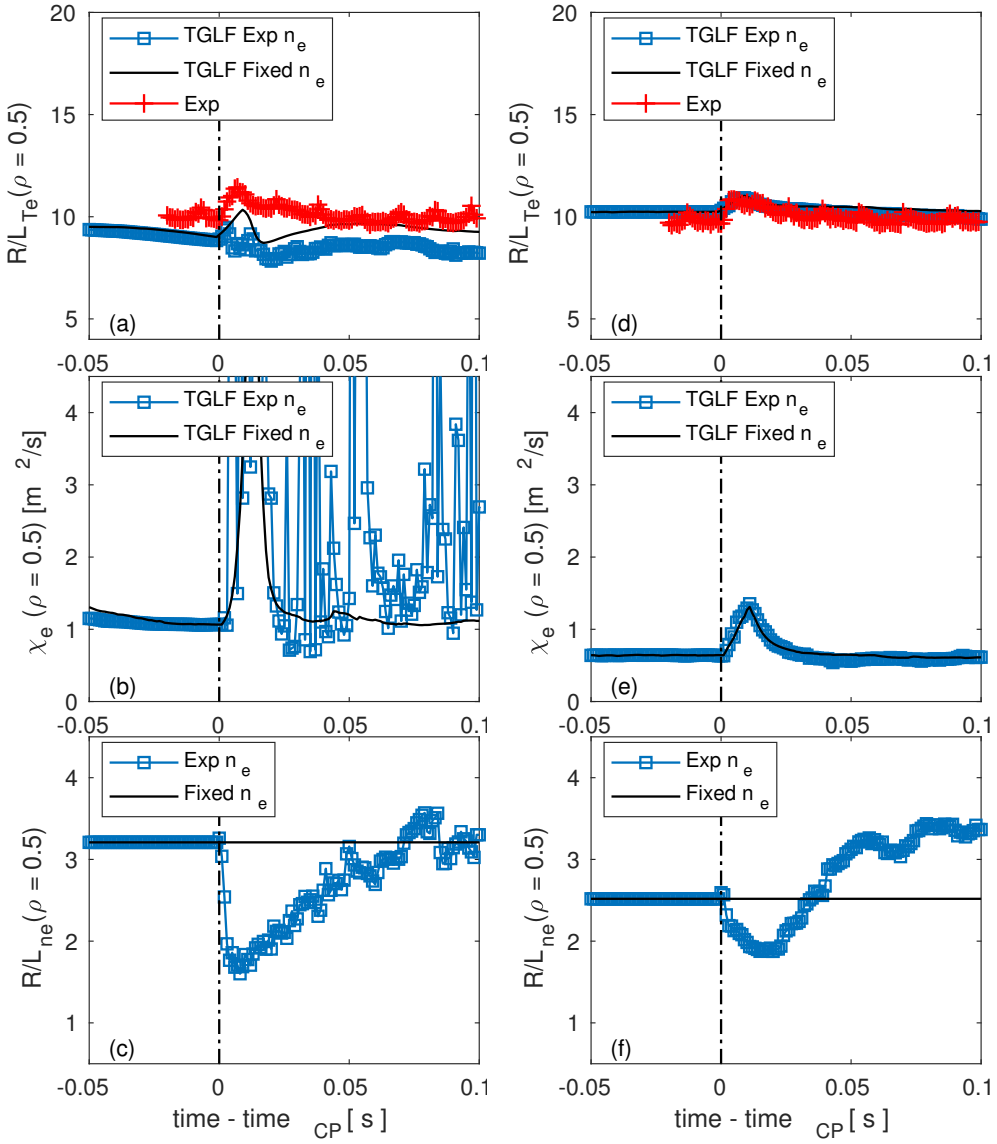

Figure 9. Time evolution of the normalized logarithmic electron temperature gradient at mid-radius ($\rho_\phi = 0.5$) obtained in the ASTRA / TGLF simulations (a,d) with prescribed density which follows the experimentally measured time evolution (squares) and which is kept fixed to the measured profile before the cold pulse (solid line), compared to the experimental measurements (crosses +). Corresponding evolution of the TGLF electron heat conductivity at the same radial location (b,e) and prescribed electron density logarithmic gradient in the ASTRA simulations (c,f). Two heating phases with large ion heating are shown, a low density NBI phase (a,b,c) and an intermediate density OH phase (d,e,f).

follows the lines of that utilized in [17], where only the electron and ion temperature profiles are modelled. In the case of the present simulations of AUG plasmas, the electron density is directly taken from the IDA measurements. With this set of transport simulations we aim to test whether the different fast responses of the electron temperature to the peripheral cold pulse can be reproduced by a theory–based local transport model like TGLF and whereas the measured density behavior, used as input in the simulations, leads to predictions which are at least qualitatively consistent with the observed electron temperature dynamical response. In this first set of simulations we impose the boundary condition at $\rho_\phi = 0.88$ and we use 112 points in the radial direction. The TGLF transport model is called every 1 ms of simulated time in the simulation, whereas the time step in the solution of the transport equations is 0.1 ms. The cold pulse is produced by a sudden increase of the radiated power at the edge, with a Gaussian profile shape centered at $\rho_\phi = 0.85$ and with a width of $\Delta\rho_\phi = 0.05$, which mimics standalone results obtained from STRAHL. The amount of total radiated power is set in order to approximately match the experimentally observed drop of the electron temperature at the periphery. As in this set of simulations the density profile is not modelled, no increase of the impurity concentration at the periphery has been included either, and the impurity content is based on the experimental effective charge number $Z_{\rm eff}$, assuming boron as only impurity, and with an impurity density profile which is proportional to the electron density profile. At the same time, in the simulations with prescribed evolving density profile, the measured variation of the electron density, which in the experiment is caused by the additional peripheral particle source provided by the impurity laser ablation, is consistently taken into account in the ASTRA transport equation for the energy conservation law, in both the time derivative $\partial n_\sigma T_\sigma/\partial t$ and the heat flux $-n_\sigma \chi_\sigma \partial T_\sigma/\partial r$, with σ the species index for electron and main ions, and where the deuterium density is computed by quasi–neutrality.

Four representative experimental phases have been considered, low density with OH and ECRH, low density NBI heated and intermediate density OH. Every heating phase has been modelled with two ASTRA simulations, one in which the electron density is made evolve following the IDA electron density profile measurements and one in which the electron density is kept fixed to the profile measured before the cold pulse injection.

The results are presented in Fig. 8 for the low density phases with OH and ECRH, and Fig. 9 for the low density phase with NBI heating and for the OH intermediate density phase. In Figs. 8(a,d) and 9(a,d) the normalized logarithmic gradients of the electron temperature profiles at mid-radius from the measurements (crosses +) are compared with those predicted by the simulations with density profiles which follow the experimental evolution (squares) or are kept fixed at the values just before the cold pulse injection (solid line). In Figs. 8(b,e) and 9(b,e) the corresponding TGLF electron heat conductivities at the same radial location are shown, while in Figs. 8(c,f) and 9(c,f) the time evolutions of the prescribed logarithmic gradients of the electron density profiles are plotted.

We observe that in the cases with dominant electron heating, Fig. 8, in the simulations with prescribed evolving electron density profile (squared), in

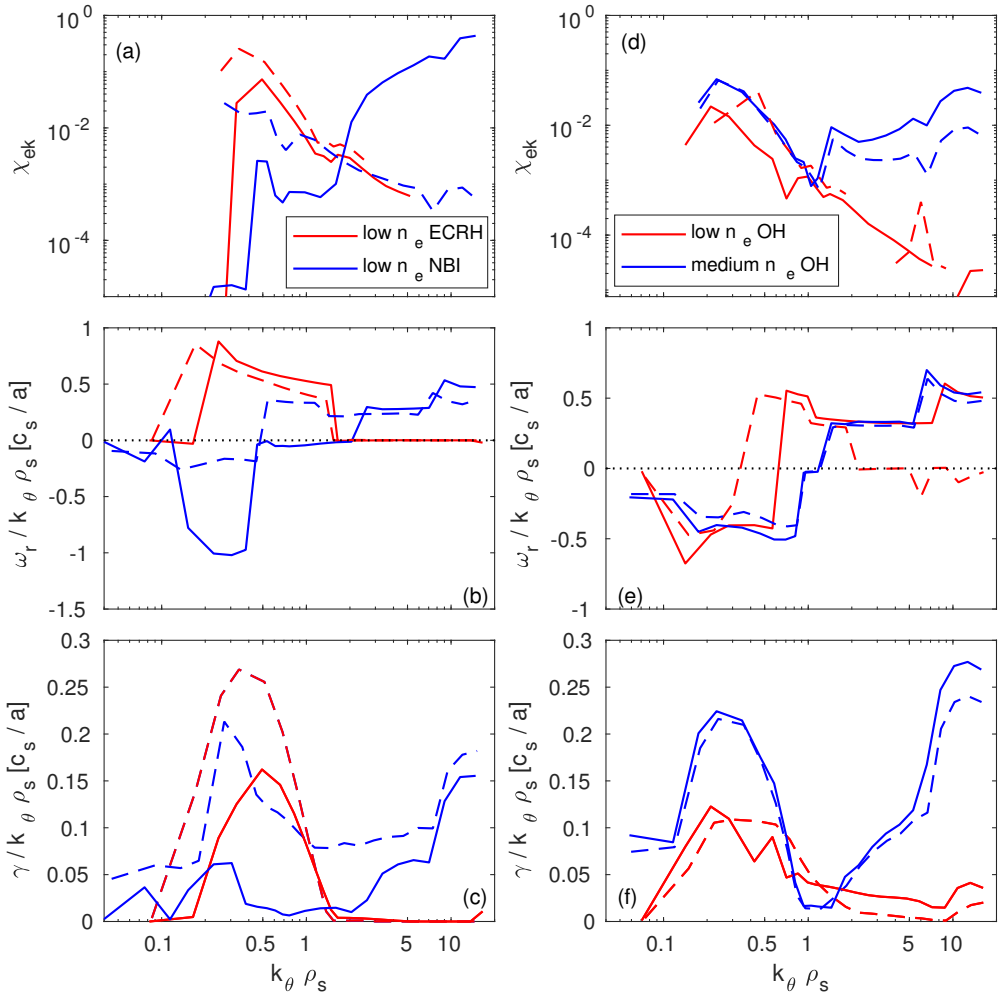

Figure 10. Binormal wave number spectra obtained from TGLF at $r/a = 0.5$ of the electron heat conductivity (a,d), real frequency (b,e) and growth rate (c,f), both normalized to the wave number, of low density ECRH and NBI heated phases (a-c) and OH phases at low and intermediate density (d-f). Solid and dashed lines show spectra 20 ms after and just before the modelled cold pulse, respectively.

correspondence to the fast experimentally measured drop of the electron density gradient, which is prescribed in the simulations, the electron heat conductivity also rapidly drops, leading in both cases to an increase of the predicted logarithmic electron temperature gradient R/L_{Te}, by an amount that approximatively matches the increase observed in the experiment. In contrast, in the simulations with electron density kept fixed at the measured profile before the cold pulse (solid lines), the electron heat conductivity does not exhibit any change in time, and the predicted R/L_{Te} does not show any significant increase, neither the central electron temperature, in clear disagreement with the experiment. We conclude that the observed sudden density flattening produced by the impurity injection causes an extremely fast reduction of the TGLF predicted electron heat conductivity, with a consequent very fast increase of the peaking of the electron temperature profile, consistent with the experimental observations. The results

also highlight the critical role of the logarithmic density gradient, rather than the density itself, because, after the start of the laser ablation, the gradient exhibits the fastest and largest variation. In contrast the density changes on a longer time scale and with a more limited variation. Thereby the fast reaction of the electron temperature demonstrates the strong sensitivity of the transport to the density gradient, rather than just to the density itself, for which the temperature reaction would be slower. The flattening of the density profile is a necessary ingredient to obtain the reduction of the heat conductivity, as simulations in which the density profile is kept constant in time do not exhibit any phase of reduced transport. This result, obtained from the modelling of the AUG results is completely consistent and fully confirms the results obtained in the recent TRANSP / TGLF modelling of the C-Mod cold pulse experiments [17, 18], and the more recent modelling activity on DIII–D plasmas [22].

In contrast, the cases with larger amount of ion heating, Fig. 9, show a completely different time evolution, although in both cases the density profile exhibits a transient flattening (although reduced in the intermediate density phase). In the low density case with NBI the sudden flattening of the electron density profile produces a fast average increase of the electron heat conductivity at mid–radius, with some intermettency in time, while the intermediate density phase shows a limited variation with a slight transient increase. As a consequence of these responses of the electron heat conductivity, which do not exhibit any strong and fast reduction, completely different from the previous electron heated cases, the predicted R/L_{Te} shows limited variations, and very similar behaviour with evolving and constant prescribed density profiles, well consistent with the experimental observations.

We conclude that, in agreement with [17, 18, 22], the electron density flattening produced by the laser blow off of the impurity is a necessary but not sufficient ingredient to obtain the fast increase of the electron temperature peaking and thereby the central increase in correspondence of the peripheral drop. In order to understand why in conditions with dominant electron heating, the electron heat conductivity decreases as a consequence of the density flattening, while in the other conditions it increases, it is of interest to investigate the turbulent regimes which are predicted by TGLF in the different heating phases. These can be expected to be realistic as they are found to lead to predictions of transport which have such a general consistency with the experimental observations.

To this end, the binormal wave number spectra of the electron heat conductivities and of the corresponding real frequencies and growth rates of the unstable modes before (dashed lines) and 20 ms after the cold pulse injection (solid lines) are presented in Fig. 10 at the radial position $\rho_\phi = 0.46$ (that is $r/a \simeq 0.5$). In Fig. 10(a-c) the low density ECRH and NBI heated phases are compared, whereas in Fig. 10(d-f) the comparison is between the OH phases at low density and intermediate densities. Both comparisons show some similar features. The low density electron heated cases (OH and ECRH) are characterized by a strong transport in the ion Larmor radius range of scales ($k_\theta \rho_s < 1$) produced by trapped electron modes (TEM), as this can be identified by the positive values of the real frequencies. In contrast, in the same range of ion scales, the phases

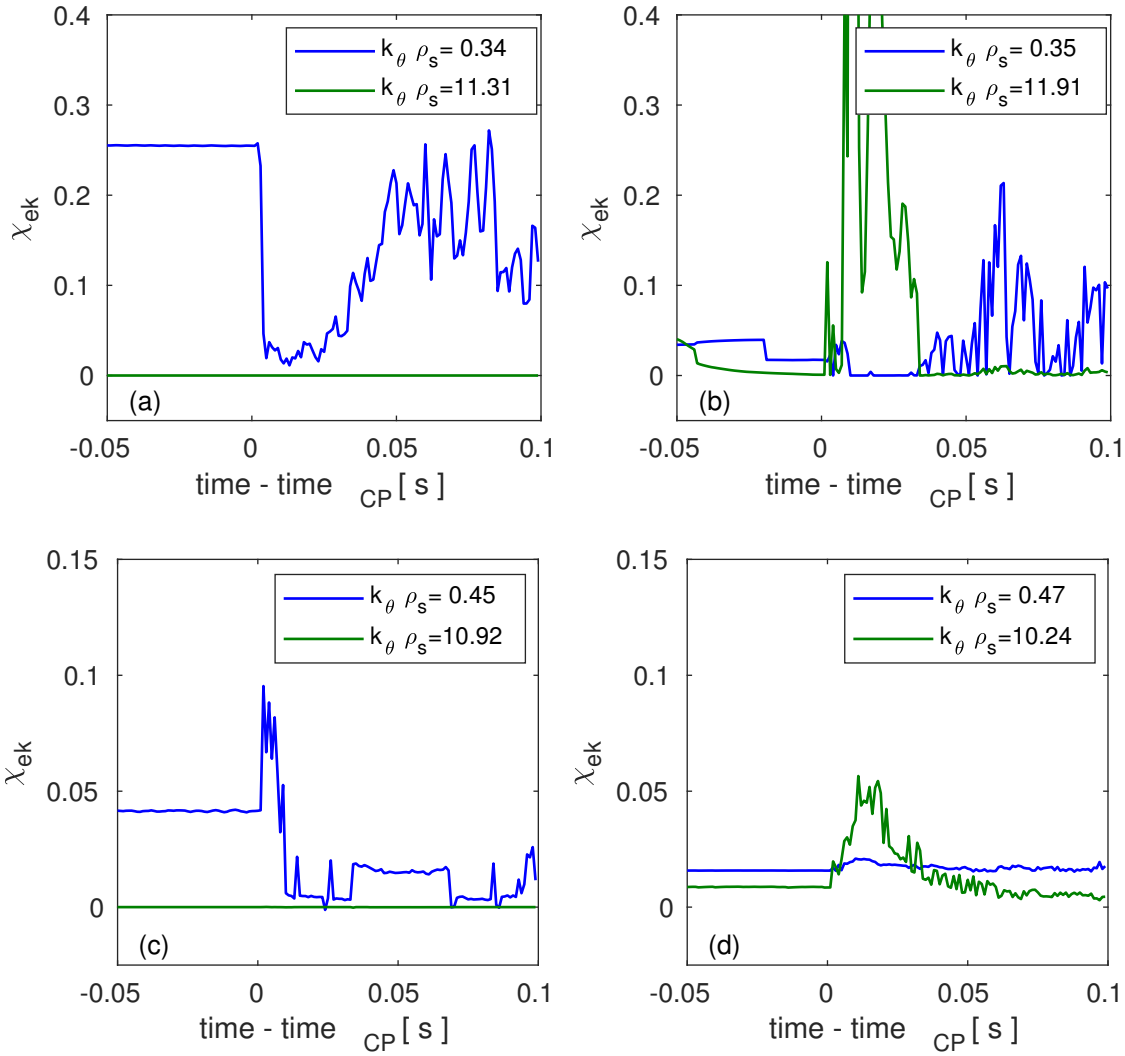

Figure 11. Time evolution of electron heat conductivity predicted by TGLF at two representative binormal wave numbers at ion and electron scales at $r/a = 0.5$, for low density ECRH (a) and NBI heated (b) phases, as well as OH phases at low (c) and intermediate (d) densities.

with larger ion heating (NBI heated at low density and OH at intermediate density) are characterized by ion temperature gradient modes (ITG). Interestingly these phases also have unstable electron temperature gradient (ETG) modes at electron Larmor radius scales ($k_\theta \rho_s > 2$). After the cold pulse injection, phases at low density are characterized by a strong reduction of the heat conductivity at ion Larmor radius scales, corresponding to a stabilization of the mode growth in that spectral range, produced by the strong reduction of the logarithmic density gradient. This is not obtained in the intermediate density phase, where the higher collisionality implies that the impact of the reduced density flattening on the growth rate is much weaker.

The low density NBI heated phase also features a reduction of the electron heat transport at ion scales, but it is also characterized by a very strong increase of the electron heat transport produced by ETG modes, produced by the reduction of T_e/T_i

and of R/L_n caused by the cold pulse. Interestingly, as a consequence of the TGLF–SAT1 multi–scale saturation rule [20, 21], a strong ETG contribution to the electron heat conductivity is produced by TGLF when the growth rate normalized to the wave number $\gamma_k/k_\theta\rho_s$ at electron scales is larger than the corresponding peak at ion scales. In the NBI heated phase this occurs only after the start of the cold pulse, but not before, although in the latter condition the ETG growth rate is higher. We have to also mention that for the low density NBI heated phase just before the laser ablation, TGLF tends to underestimate the ion heat transport, and this delivers ratios of T_e/T_i in the simulation which are lower than in the experiment. This feature could also extend during the transient phase produced by the cold pulse, what cannot be directly verified against the experimental measurements due to the absence of time resolved ion temperature measurements in that phase, and could lead to an overestimate of the TGLF prediction of the strength of the ETG in that phase. The underprediction of the ion heat transport by TGLF was already observed in the modelling of L–mode AUG plasmas [39] and it is likely related to a too weak stiffness in the ion heat transport channel of the TGLF–SAT1 version of this transport model [40].

The different roles of the ion and electron Larmor radius scales after the injection of the cold pulse can also be observed in the time traces presented in Fig. 11, where the time evolution of selected representative wave numbers at ion and electron scales are compared. The low density ECRH phase is presented in Fig. 11(a), which shows the strong decrease of the electron heat conductivity at the ion scales, and no transport at electron scales. A similar time evolution is present in the low density OH phase Fig. 11(c). In contrast, the low density NBI phase in Fig. 11(b) displays a strong increase of the ETG transport after the cold pulse injection, still combined with a reduction of the electron heat transport produced at ion scales. Finally, the OH phase at higher density is characterized by the absence of a reduction of the electron heat transport at ion scales concomitant to an increase of the transport at electron scales.

We conclude that the electron to ion temperature ratio T_e/T_i plays a critical role in determining the realtive importance of the opposite, stabilizing and destabilizing, effects caused by the reduction of the normalized logarithmic density gradient R/L_n on modes at ion and electron scales respectively. Conditions characterized by large values of T_e/T_i are not affected by strong ETG transport and profit of the suddden reduction of R/L_n produced by the impurity laser ablation for a fast and strong reduction of the electron heat conductivity at ion scales, and the consequent increased electron temperature peaking, with a central increase of the electron temperature rapidly following the drop at the edge. Conditions characterized by values of T_e/T_i close to one are strongly affected by an increase of the ETG transport caused by the reduction of R/L_n produced by the impurity ablation, thereby not leading to any overall reduction of the electron heat conductivity nor to an increase of the electron temperature peaking. In agreement with [17,18,22], the sudden flattening of the electron density profile in combination with the complex impact that this has on the different turbulence regimes, as described by a local model of turbulent transport like TGLF, is able to explain the different responses of the electron temperature profile observed in the different operational conditions. In

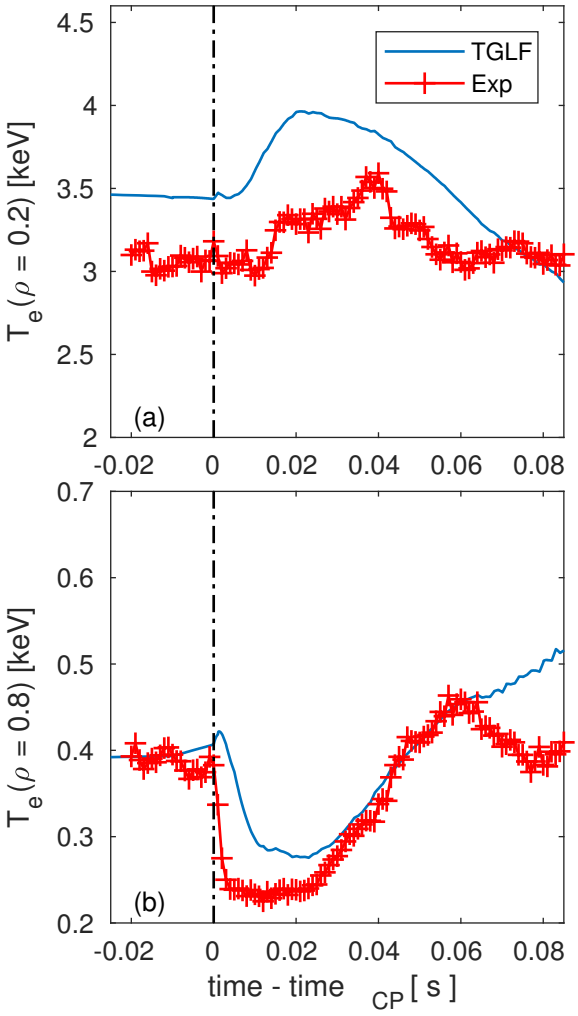

Figure 12. Time evolution of the central (a) and peripheral (b) electron temperature in a ASTRA/STRAHL/TGLF simulation with 8 10^{21} injected impurity atoms per second and an impurity diffusion coefficient $D_Z = 0.3\chi_i$.

particular the consistency in the physical behaviour between the observations in OH phases and in phases with auxiliary heating is pointed out here for the first time.

4. Transport modelling with predicted electron density

The remaining key, yet unanswered, question is of course related to the explanation of the sudden flattening of the density profile as a consequence of the impurity laser ablation. Can this extremely fast response be still modelled and explained within a local transport model, or, does this plasma dynamical response require a non-local transport mechanism?

In order to answer to this question, we extend the ASTRA TGLF transport modelling to also simulate the particle densities. We make use of the coupling between ASTRA and the impurity transport code STRAHL [28, 29]. STRAHL is used to model the carbon laser blow off and to compute the time evolution of the impurity density. On

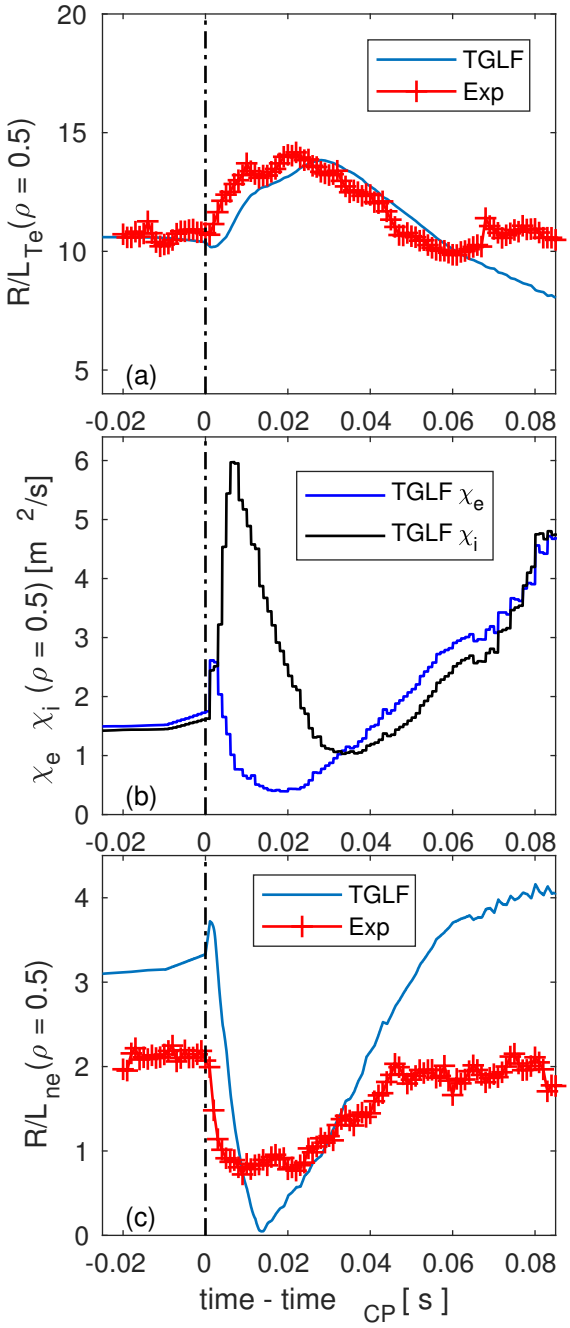

Figure 13. Time evolution of the normalized logarithmic electron temperature gradient R/L_{Te} (a), electron and ion heat conductivities (b) and normalized logarithmic electron temperature gradient R/L_{ne} (c) at mid–radius in the same simulation of Fig. 12.

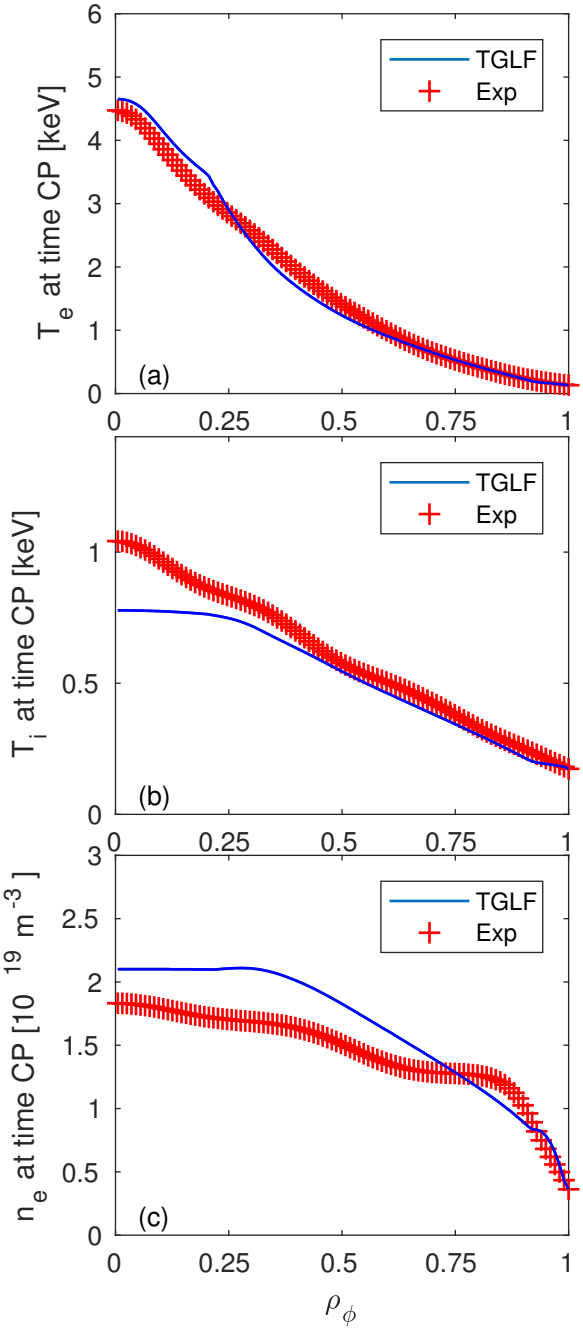

Figure 14. Profiles of electron temperature (a), ion temperature (b), and electron density (c) in stationary conditions, before the application of the laser ablation in the simulation, with comparison to the corresponding electron temperature and density measurements from IDA (a,c) and ion temperature with CXRS (b).

the ASTRA transport side the density of the main ions, deuterons, is evolved with the TGLF predicted main ion particle flux, and the TGLF calculations include the ablated carbon impurity density as kinetic species and thereby the impact that this has on the turbulent transport also of the main species. The electron density is then computed in ASTRA by quasi–neutrality. Since in these simulations the entire impurity ablation process is modelled with STRAHL, the boundary condition is moved to the edge of the plasma $\rho_\phi = 1$, with a radial discretization of 129 grid points. The process of the laser ablation is modelled by providing to STRAHL a time dependent boundary condition at the periphery of the domain (corresponding to $\rho_\phi = 1$) by which, for a short time window, the arrival of an increased amount of carbon atoms is imposed. A difficulty which has been encountered in these highly integrated transport simulations is that the inclusion of the turbulent carbon impurity flux predicted by TGLF as transport component in STRAHL, in addition to the neoclassical impurity transport computed with NCLASS, delivers highly unstable simulations, which do not allow us to reach a well converged time evolution of the modelled densities and temperatures of the various species. This can be understood by the fact that, differently from ASTRA, STRAHL is not a transport code optimized for stiff transport models. In order to consistently keep the modelling of the carbon density evolution within STRAHL, during the phase of the laser ablation, we have adopted the solution of including in STRAHL a turbulent diffusivity for carbon which is proportional to the TGLF predicted ion heat conductivity. As it will be presented later, stand-alone calculations with TGLF have shown that this is a reasonable physical approximation. By the inclusion of this component of the impurity transport, the simulation resulted stable in time, delivering well reproducible time evolutions of the kinetic profiles. For these more complete simulations, which also include the density evolution, and specifically aim at testing whether also the fast density response can be predicted by a local theory–based transport model, we focus on the modelling of the cold pulse in a phase at low density with ECRH. This is the phase which exhibits the strongest increase of the central electron temperature, also in combination with a very strong and fast flattening of the electron density profile. The results of a first simulation are presented in Fig. 12, Fig. 13 and Fig. 15. This simulation is obtained with the boundary condition that the laser ablation produces 8 10^{21} atoms of carbon per second in the time window of 10 ms at the periphery of the simulated domain. The corresponding peak in total radiated power produced by the carbon ablation in the simulation reaches 900 kW before 10 ms after the start of the laser ablation. This is roughly consistent with the upper bound of a range between 300 kW and 800 kW which can be inferred from the deconvolution of the measurements of the edge diode bolometers. These values also reproduce relatively well the observed temperature drop at the edge. This first simulation demonstrates that a central increase of the electron temperature is obtained corresponding to a reduction at the edge which quantitatively follows the time evolution which is experimentally observed also when the particle densities are dynamically predicted. The corresponding time evolution of the normalized electron temperature and density logarithmic gradients at mid–radius are compared with the experimental measurements in Fig. 13. This simulation also

demonstrates that the local theory–based transport model TGLF can reproduce a sudden reduction of the electron density gradient at mid–radius as a consequence of an impurity laser ablation at the edge, consistent with the experimentally observed very fast reponse. We also notice that the values of R/L_n predicted by TGLF is higher that the one experimentally reconstructed by IDA, and that the simulated amount of flattening is larger than the one experimentally observed. A comparison of the predicted profiles just before the start of the laser ablation process in the simulation is presented in Fig. 14, which shows that TGLF can produce realistic predictions of the electron and ion temperature profiles, as well as of the electron density, although the latter more peaked than what is experimentally observed. We also notice that, similarly to the simulations with prescribed evolution of the electron density, the electron heat conductivity decreases as a consequence of the reduction of the normalized electron density logarithmic gradient R/L_{ne}. However, an interesting feature of these complete simulations which also evolve the particle species is that transiently, after the start of the laser ablation, the ion heat conductivity is found to strongly increase. In order to better understand the reasons behind this transient increase of the ion heat conductivity and its impact on the dynamics of the profiles developed by these transport simulations, in Fig. 15 we show the time evolution of the most relevant kinetic profiles during the first 24 ms after the start of the laser ablation, that is over the entire phase of the central electron temperature rise obtained in the simulation. In this simulation the amount of carbon particles which has been introduced is large enough to produce transiently hollow electron density profiles, Fig. 15(a), which are not observed experimentally, Fig. 15(b). At this stage, however, the point of this simulation is to investigate whether a fast inward propagation of the particles is indeed possible within a local transport description. We shall provide later the example of another simulation in which no hollow density profile has been obtained, still reproducing all of the qualitative features of the experiment. We also observe that the carbon density profiles transiently develop strongly hollow profile shapes, as shown in Fig. 15(c), as the ionization and fast inward propagation of the laser ablated carbon also produces the fast variation of the electron density profile, which tracks that of the impurity, as shown in Fig. 15(b), while leaving the density profile of the deuterons almost unchanged, Fig. 15(d). Interestingly, this simulation also produces a very clear pivot point of the electron temperature profile, which remains remarkably constant in time, located around mid–radius, as shown in Fig. 15(e), with a central increase of the electron temperature which reaches the 600 eV for a maximum drop at the edge of less than 200 eV. We also observe that the time window over which the impurity density profile is reversed corresponds to that over which an increase of the ion heat conductivity is obtained, as it can be observed in the time evolution of all of the gradients at the radial location $\rho_\phi = 0.56$ Fig. 15(g) and the corresponding heat conductivities at the same location Fig. 15(h).

The fast inward propagation of the carbon impurity ions also produces a fast variation of the electron density profile Fig. 15(a,f), which consequently leads to the reduction of the electron heat transport and to the increase of the peaking of the electron temperature profile. The transient strongly reversed density profiles of carbon produce

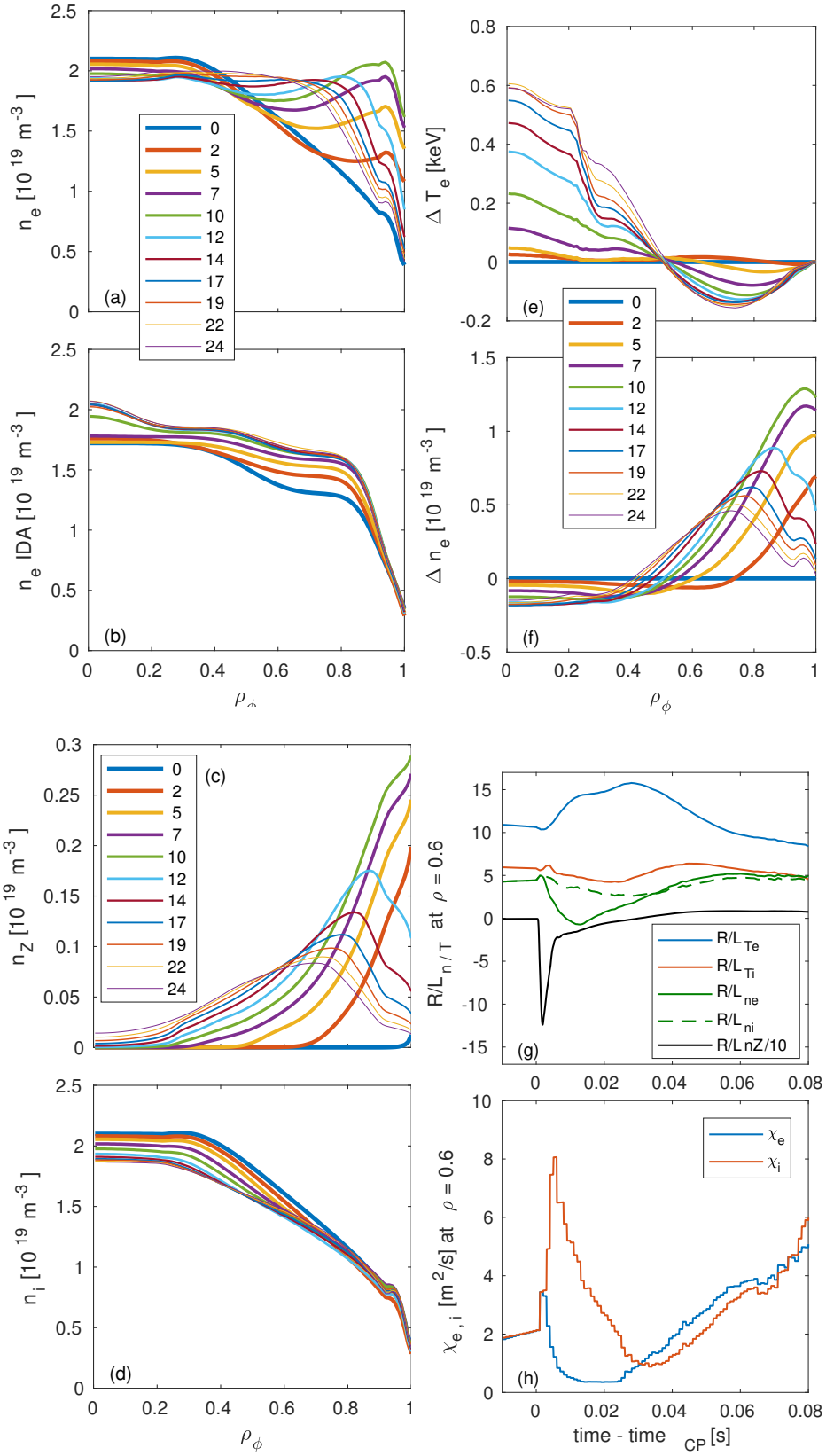

Figure 15. Time slices of the evolution of the predicted (a) and measured (b) electron density, predicted impurity density (c), predicted deuterium density (d) as well as variation of the predicted electron temperature (e) and electron density (f). Time evolution of the normalized logarithmic gradients of the electron and ion temperatures, and particle densities at $\rho_\phi = 0.6$ (g) and corresponding time evolution of the electron and ion heat conductivities at the same radial location. The impurity diffusion coefficient is $D_Z = 0.3\chi_i$. Values in the legends indicate the time interval in ms after the start of the laser ablation corresponding to each profile in the plot.

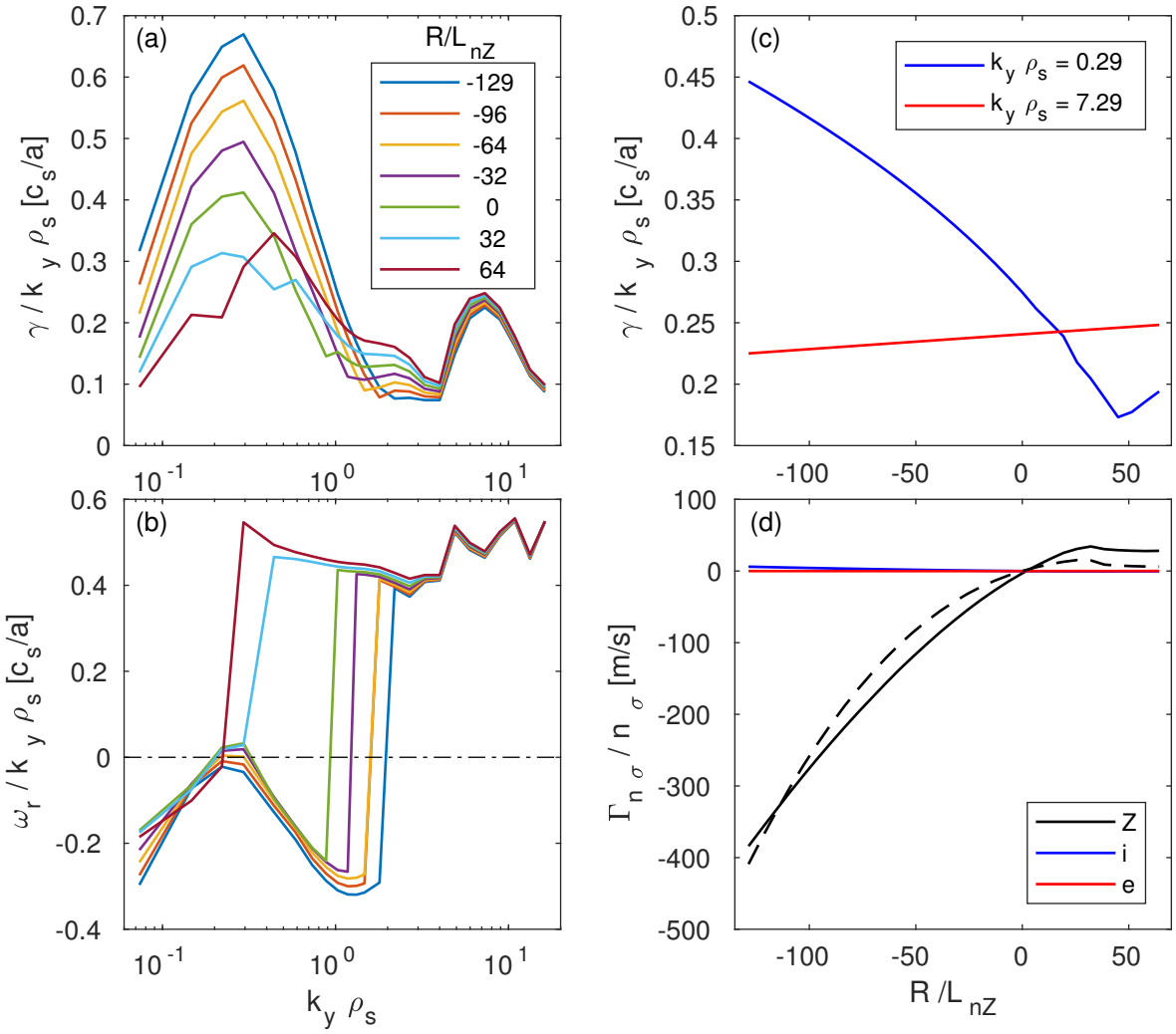

Figure 16. TGLF spectra of the growth rate (a) and real frequency (b), both divided by the normalized binormal wave number, as a function of the normalized binormal wave number for different values of the normalized logarithmic density gradient of the carbon impurity density R/L_{nZ} as reported in the legend in (a). TGLF growth rates, divided by the normalized binormal wave number, for two values of the binormal wave number as reported in the legend (c) and TGLF particle fluxes of carbon, deuterium and electron (Z, i, and e in the legend) (d) as a function of R/L_{nZ}. The dashed curve in (c) shows the particle flux of carbon obtained assuming the carbon diffusivity D_Z to be $D_Z = 0.6\chi_i$, with χ_i the main ion heat conductivity.

locally normalized logarithmic gradients which are extremely large in absolute value. These gradients are found to destabilize a mode in the ion diamagnetic direction which can be identified as an impurity density gradient driven mode. This is demonstrated in Fig. 16 where, starting from the local conditions at $\rho_\phi = 0.56$ obtained in the ASTRA/STRAHL/TGLF simulation, precisely 5 ms after the start of the carbon laser ablation, a scan in the normalized logarithmic gradient of the carbon density R/L_{nZ} is performed with TGLF in stand–alone mode (at that time slice, $R/L_{nZ} = -80.5$ in the ASTRA/STRAHL/TGLF simulation). In Fig. 16(a,b) the spectra of the

growth rate and real frequency are shown, which identify a mode in the ion Larmor range which propagates in the ion diamagnetic direction (negative values of the real frequency in TGLF sign conventions) and which has a growth rate which increases with increasing absolute value of R/L_{nZ}, Fig. 16(c). This mode produces a very large inward particle flux of carbon impurity ions, Fig. 16(d), which strongly increases with increasing $-R/L_{nZ}$, and thereby can be mainly considered to be of diffusive nature. For this reason, given that the combined ASTRA/STRAHL/TGLF simulations turned out to be strongly unstable when directly giving this impurity flux as input of the impurity transport code STRAHL, it has been taken the simplification of parametrizing this inward flux as produced by an impurity diffusion coefficient proportional to the ion heat conductivity, an approximation which provides a reasonable description of the particle flux versus density gradient relationship of the impurity, as shown in Fig. 16(d), where the dashed curve has been obtained assuming $D_Z = 0.6\chi_i$. Of course, this simplification completely remains within the description of a local transport model. **At the same time, this prediction of an inward, mainly diffusive, turbulent flux of impurities predicted by TGLF motivates a comparison and a verification against gyrokinetic predictions of impurity transport in these plasma conditions, which are currently planned as future work**. In the simulation presented in Fig. 12, Fig. 13 and Fig. 15, a coefficient $D_Z = 0.3\chi_i$ has been included in STRAHL, which has ensured a good stability of the simulated time evolution of the cold pulse. A reduction by 25% of the amount of carbon atoms which are injected by the laser ablation, that is, 6 10^{21} atoms of carbon per second in the time window of 10 ms, combined with an increase of the carbon diffusivity to $D_Z = 0.50\chi_i$ yield a simulation in which the transient variation of the electron density profile does not lead to locally hollow electron density profiles, more consistent with the experimental observations, still with a sudden reduction of the electron density gradient over a large portion of the minor radius, and a corresponding very fast increase of the central electron temperature, even faster than what is experimentally observed. The time traces of this simulation are presented in Fig. 17 and Fig. 18, where also a comparison with a corresponding simulation in which the impurity diffusion coefficient has been reduced and taken proportional to the electron heat conductivity is presented. The results of the simulation with reduced amount of injected particles and increased impurity diffusivity (more consistent with the TGLF impurity flux), which are presented in Fig. 17 and Fig. 18 (a-c), in comparison to those shown in Fig. 12 and Fig. 13 exhibit the same qualitative features, with quantitative differences in the amount of density flattening and the speed of the dynamical response. A comparison of the time evolution of the kinetic profiles can be obtained from Figs. 19 and 15. **We observe that in both simulations presented in Figs. 13 and 18(a-c), the reduction of the electron density logarithmic gradient R/L_{ne} is larger than what is experimentally observed. The predicted value of R/L_{ne} at mid–radius before the cold pulse is higher than the value obtained by the IDA reconstruction of the experimental electron density profile. At the same time, the simulation with reduced amount of injected impurities reaches minimum values of R/L_{ne} after the cold pulse which are in**

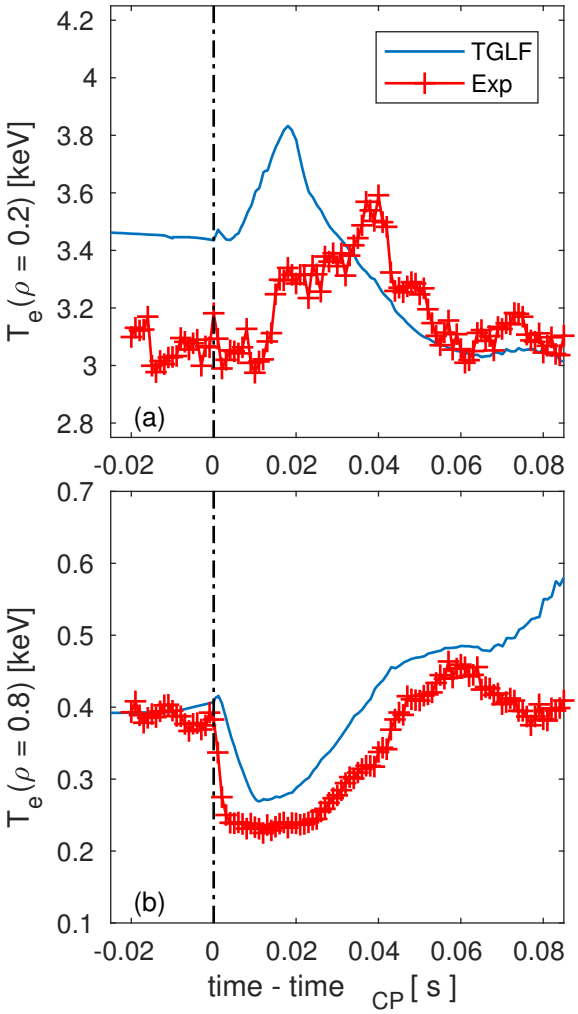

Figure 17. The same as in Fig. 12, this time from a simulation with reduced amount of injected impurity atoms (6 10^{21} atoms/s) and increased diffusion coefficient $D_Z = 0.5\chi_i$.

good agreement with those obtained by the IDA reconstruction, as shown in Fig. 18(c). This shows that the impurity ablation and consequent impurity transport can produce a flattening of the density profile which is compatible with the observations, and further demonstrates, in agreement with the ASTRA/TGLF simulations with prescribed density profiles presented in Section 3, that the level of density flattening obtained in the experiment is consistent with the required stabilizing effect on the electron heat transport to produce a central increase of the electron temperature.

In contrast, the results of the simulation with reduced impurity diffusivity presented in Fig. 18 (d-f) exhibit a completely different qualitative behaviour. In this case the impurity diffusivity has been assumed to be $D_Z = 0.5\chi_e$, and thereby significantly smaller than in the previous cases and in particular without the strong transient increase after the start of the cold pulse which is predicted by TGLF, which is also reflected in the strong transient increase of the ion heat conductivity, Fig. 13(b) and 18(b). With

such a reduced inward diffusion of the impurity, the dynamics of particle transport after the start of the impurity ablation, and in particular the density flattening at mid–radius take place on a longer time, also much longer than in the experiment. The achieved minimum value of logarithmic density gradient is also significantly larger. Consistent with the results presented in Section 3, this unavoidably leads to a weaker stabilization of the TEM turbulence, and thereby to no increase of the logarithmic gradient of the electron temperature (and thereby neither a central increase of the temperature) in clear contrast with the experimental observations. This test case with reduced impurity diffusion demonstrates the importance of the fast penetration of the impurity, which is accelerated by the destabilization of the impurity driven mode identified in Fig. 16, and which occurs in the phase with strong reversed profiles of the impurity density in the plasma region outside mid–radius.

The sensitivity on both the amount of injected particles and the strength of the inward impurity diffusion allow us to conclude that all of the observed phenomenlogy can be realistically reproduced by means of a completely local transport model. The experimental observations of sudden flattening of the electron density profile and the fast central increase of the electron temperature in response to the impurity laser ablation are quantitatively compatible with the predictions of the local theory–based transport model TGLF.

5. Summary and conclusions

A set of experiments have been performed in ASDEX Upgrade in order to characterize the plasma response to cold pulses, produced by laser ablation of a light impurity, in conditions of dominant electron and ion heating, complementing the large amount of investigations performed in the past which focused on the impact of an increase of the plasma density, often under Ohmic heating only. The well–known rapid increase of the central electron temperature following the drop at the periphery regularly observed at low density, is shown to only occur in conditions in which the electron heat flux is dominant. Plasmas at the same low density, but with a large amount of ion heating, do not exhibit this peculiar behaviour. At higher density, no increase of the central electron temperature is observed as a consequence of a cold pulse at the edge, consistent with past observations. These experimental results more clearly relate the plasma response to the electron and ion heat flux levels present in the plasma, rather than to the actual plasma density, and thereby directly point to a connection between the plasma behaviour and the type of turbulence which is present in the plasma. This is strongly regulated by the electron to ion temperature ratio, which is directly reflecting the electron to ion heating ratio which is present in the plasma. Consistent with recent experimental and modelling results obtained in C-Mod [17, 18] and DIII–D [22], in all conditions explored in the AUG experiments, a sudden flattening of the density profile over a wide radial domain is observed as a consequence of the impurity laser ablation, more pronounced at low density. The flattening of the density profile plays a critical role in the modification of the turbulence after the start of the laser ablation. In

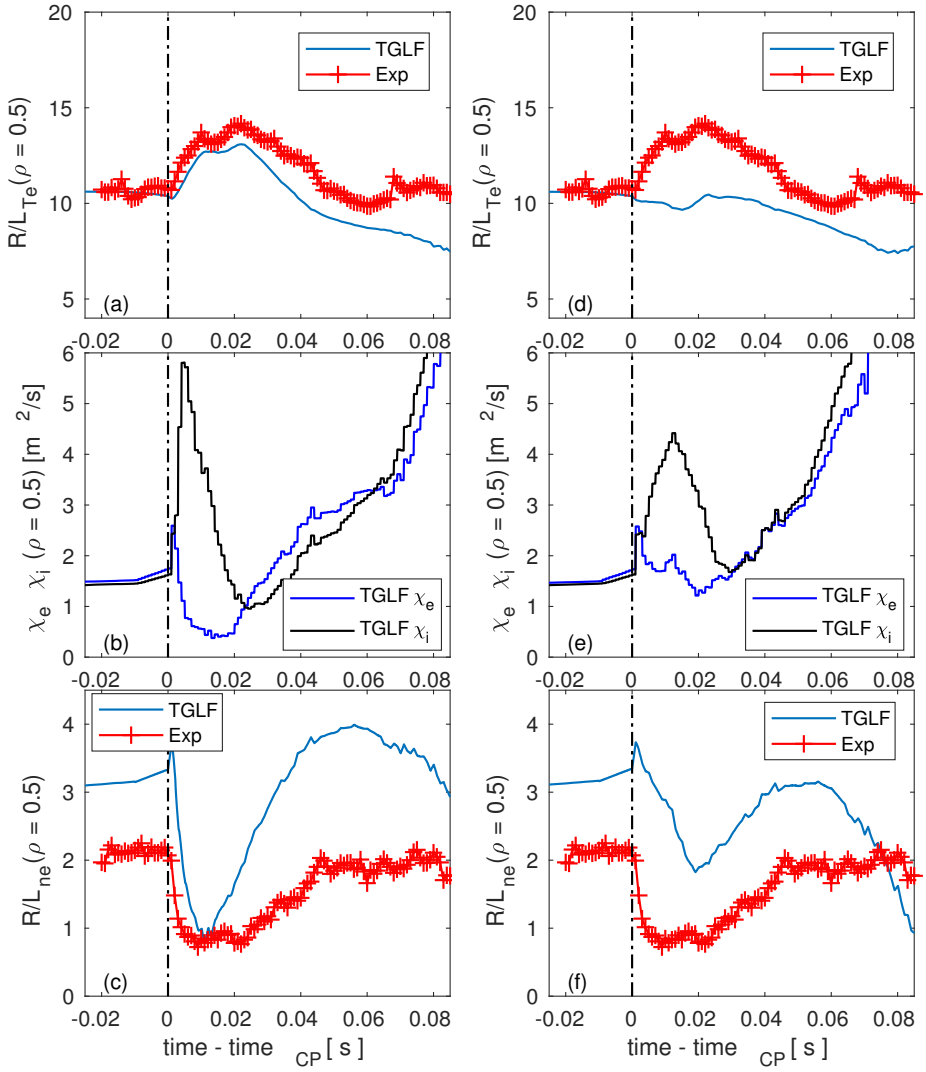

Figure 18. Comparison of the time evolution of the normalized logarithmic temperature gradient R/L_{Te} (a,d), the ion and electron heat conductivities (b,f) and normalized logarithmic electron density gradient R/L_{ne} (c,e) in the case the impurity turbulent diffusivity is $D_Z = 0.5\chi_i$ (a,b,c) and in the case $D_Z = 0.5\chi_e$ (d,e,f)

conditions in which the electron heat flux dominates, characterized by a large ratio of T_e/T_i, the turbulence is mainly produced by TEM, which are strongly stabilized by the sudden reduction of the logarithmic density gradient. The consequent rapid drop of the electron heat conductivity allows the increase of the logarithmic gradient of the electron temperature, what explains the increase of the central electron temperature directly following the drop at the edge observed in these conditions. In contrast, in conditions with large ion heating, and $T_e/T_i \approx 1$, even at equally low density, the flattening of the electron density gradient leads to an increase of the ETG driven transport, which does not lead to any reduction of the electron heat conductivity, neither a fast increase of the electron temperature in the core, consistent with the observations. Transport modelling with ASTRA and the TGLF transport model, with prescribed density profiles

which follow the experimentally measured evolution, reproduce all of the features of these observations, to large extent even quantitatively. This demonstrates that the experimentally measured modifications of the electron density profile are compatible with the theoretical explanation of the different responses of the electron density in the different heating scenarios. The same transport simulations, but performed with constant in time density profiles, are unable to reproduce the observations, and in particular do not produce any increase of the central electron temperature in conditions of dominant electron heating, in clear disagreement with the experiment. This clearly identifies the key role of the electron density flattening in determining the response of the electron temperature in conditions of dominant electron heating. These results are fully consistent with the results presented in [17, 18] for C–Mod and [22] for DIII–D, and demonstrate that the physics explanation provided in those works also applies to ASDEX Upgrade. The present results also demonstrate that the electron density profile measurements are compatible with theory–based predictions of the temperature profile which are consistent with the experimental observations, and extend previous results obtained for OH to plasma conditions with auxiliary electron and ion heating. As a new element, the comparison between plasmas with auxiliary electron and ion heating clearly identifies the critical role played by the eletron to ion temperature ratio T_e/T_i in determining the turbulence producing the larger amount of electron heat transport, TEM at $T_e/T_i \gg 1$ and ETG at $T_e/T_i \approx 1$, and thereby also the opposite response to a flattening of the density profile, with stabilization of TEM turbulence and destabilization of ETG turbulence.

This body of consistent results obtained from observations and modelling of plasmas from three devices points to the key role of the density profile in this type of experiments. Thereby, the critical missing step, which has been undertaken in the present work for the first time, is the dynamical modelling of the density profile in the presence of cold pulses produced by laser ablation of impurities. To this end, we have shown results of an integrated modelling approach based on the coupling of ASTRA, STRAHL and TGLF, with boundary condition of the resolved radial domain at the separatrix, in which not only the electron and ion temperature are simulated, but also the main ion and the impurity densities, while the electron density is determined by quasi–neutrality. The results of the simulations demonstrate that also the very fast flattening of the density profile can be reproduced by a local theory–based transport model like TGLF. The simulations of a low density plasma with auxiliary central electron heating show that, directly after the start of the laser ablation, the strongly reversed impurity density profile which develops in the outer region of the plasma affects the turbulence, with micro–instabilities that produce a strong inward flux of the impurities, mainly of diffusive nature. This transient effect helps in producing a fast inward transport of the particles, leading to simulations which match the sudden flattening of the density profile over an extended portion of the plasma minor radius, what is required to obtain the stabilization of TEM turbulence and the rapid increase of the electron temperature in the center. The predictions obtained with the TGLF–SAT1 transport model in the ASTRA / STRAHL simulations are quantitatively compatible with the experimental observations of the time

evolution of the electron temperature and electron density obtained in ASDEX Upgrade. The comparison of the predicted dynamical evolution of the ion temperature with the experimental measurements has not been possible in this work, due to the absence of measurements of the ion temperature with high time resolution in these conditions at ASDEX Upgrade. **We underline that while the ASTRA, STRAHL and TGLF modelling presented in this work reveal that the impurity transport following the impurity laser ablation plays a critical role in the flattening of the electron density profile in these low density conditions, the impurity behaviour should not be considered an essential ingredient determining the response of the central electron temperature to a peripheral drop. Whatever type of mechanism which produces a negative perturbation of the electron temperature at the edge and, concomitantly, a sudden flattening of the electron density profile, also without any injection of impurities, should be expected and it is predicted to produce similar effects, as demonstrated by the simulations with the prescribed electron density profiles. Once again, the essential ingredient is the fast flattening of the electron density profile, regardless how this is obtained. Therefore, it would certainly be of interest to investigate the consistency of the present results, which are obtained in the modelling of experiments with impurity laser ablation, with the observations from experiments in which the edge perturbation is produced by supersonic molecular beam injection (SMBI) [41,42], in the absence of an impurity laser ablation. The comparison with these experiments, and related dedicated modelling, should allow one to assess whether also in SMBI experiments local particle transport can produce a sufficiently fast flattening of the electron density profile and consequently the required reduction of the electron heat transport, or if, at least in these experimental conditions, non–local effects have to be invoked.**

In conclusion, the present work provides an additional key element in the understanding of the physics of the plasma response to cold pulses produced by laser ablation of impurities. The peculiar phenomenology of the very fast central increase of the electron temperature in response to a drop at the edge, which has been for long considered a proof of "non–local" transport in tokamak plasmas, can be completely explained by means of the predictions of a theory–based local transport model, like TGLF, without the need of assuming any non–local transport mechanism. These results, together with those recently obtained in C–Mod [17, 18] and DIII–D [22], provide a very complete example of the complex nature of turbulent transport, where the high sensitivity on local plasma parameters combined to the multi–channel nature of the turbulence can produce very fast dynamical behaviours, still fully compatible with the description of local transport, but which can be erronously interpreted as the signature of a non–local response.

Acknowledgments The Authors are grateful to I. Faust for his assistance in the experiments with tungsten laser ablation, as well as to R. Fischer for the integrated data analysis and to R.M. McDermott for the charge exchange recombination spectroscopy

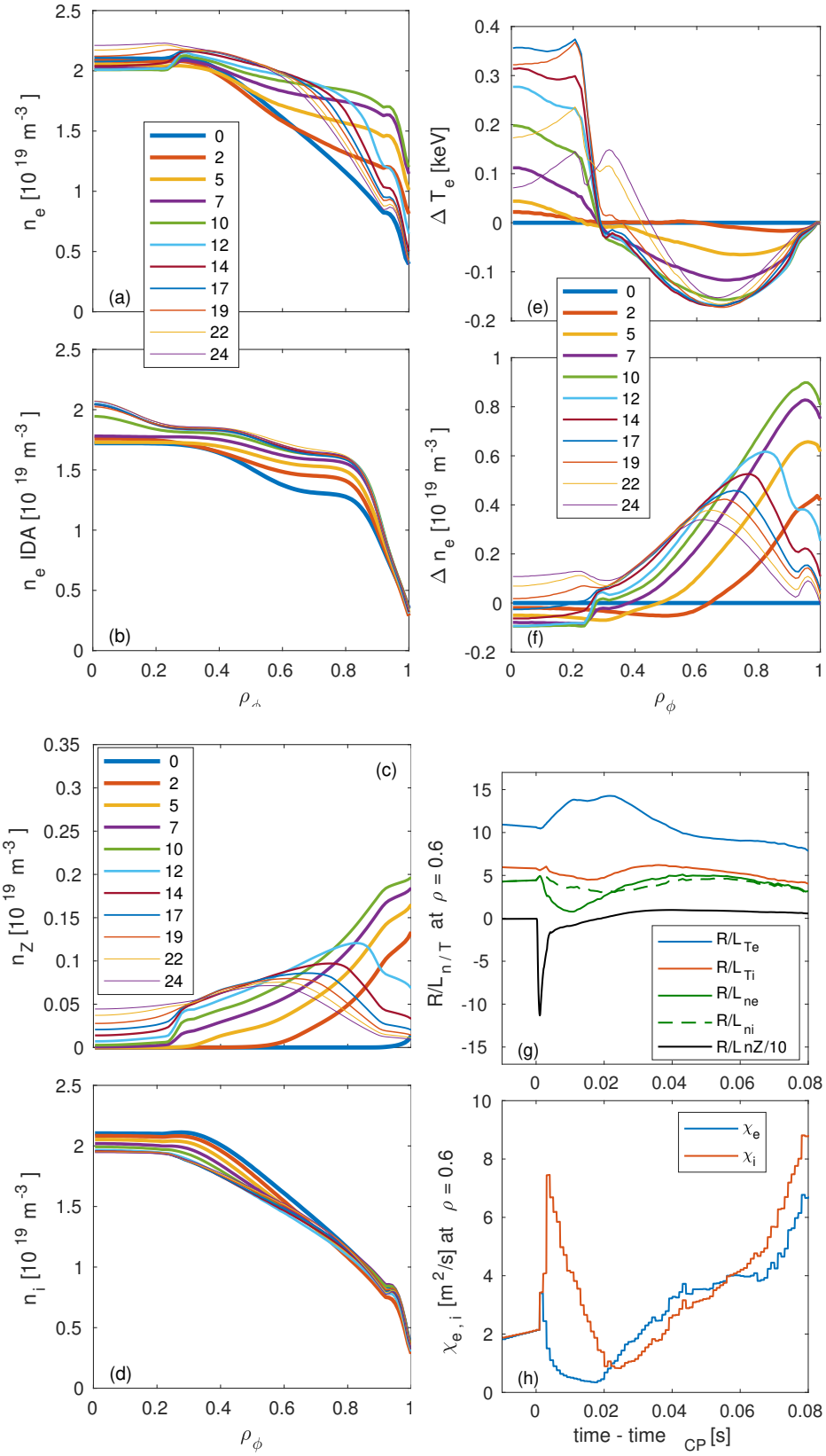

Figure 19. The same as in 15, this time for the simulation with reduced amount of injected particles and increased impurity diffusivity $D_Z = 0.5\chi_i$.

measurements used in this work. C.A. is also grateful to T. Luda di Cortemiglia, E. Trier and P. Mantica for very fruitful discussions. This work has been carried out within the framework of the EUROfusion Consortium and has received funding from the Euratom research and training program 2014-2018 and 2019-2020 under grant agreement No 633053. The views and opinions expressed herein do not necessarily reflect those of the European Commision. **P.R.F. was supported by U.S. Department of Energy, Office of Science, Office of Fusion Energy Sciences, under awards DE-SC0014264 and DE-SC0017381.**

[1] K.W. Gentle et al., Phys. Rev. Lett. 74, 3620 (1995).
[2] M.W. Kissick, J. D. Callen, E. D. Fredrickson, A. C. Janos, and G. Taylor, Nucl. Fusion 36, 1691 (1996).
[3] T. Dudok de Wit, M. Erba, M. Mattioli, and J.-L. Segui, Phys. Plasmas 5, 1360 (1998).
[4] P. Mantica, P. Galli, G. Gorini, G. M. D. Hogeweij, J. de Kloe, N. J. Lopes Cardozo, and RTP Team, Phys. Rev. Lett. 82, 5048 (1999).
[5] P. Galli et al 1999 Nucl. Fusion **39** 1355.
[6] F. Ryter et al 200 Nucl. Fusion **40** 1917.
[7] P. Mantica et al., Plasma Phys. Controlled Fusion 44, 2185 (2002).
[8] N. Tamura et al 2005 Phys. Plasmas **12** 110705.
[9] S. Inagaki et al. 2011 Phys. Rev. Lett. 107, 115001.
[10] X. R. Duan et al. 2009 Nucl. Fusion 49, 104012.
[11] J. E. Rice et al. 2013 Nucl. Fusion 53, 033004.
[12] Y. J. Shi et al. 2017 Nucl. Fusion 57, 066040.
[13] J. D. Callen and M.W. Kissick 1997 Plasma Phys. Controlled Fusion 39, B173.
[14] K. Ida et al. 2015 Nucl. Fusion 55, 013022.
[15] G. M. D. Hogeweij et al., 2000 Plasma Phys. Control. Fusion **42** 1137.
[16] J. E. Kinsey, R. E. Waltz, and H. E. St. John 1998 Phys. Plasmas **5** 3974.
[17] P. Rodriguez-Fernandez et al 2018 Phys. Rev. Lett. **120** 075001.
[18] P. Rodriguez-Fernandez et al 2019 Nucl. Fusion to be published.
[19] G. M. Staebler, J. E. Kinsey R. E. Waltz 2007 Physics of Plasmas **14** 055909.
[20] G. M. Staebler, J. Candy, N. T. Howard, and C. Holland 2016 Phys. Plasmas **23** 062518.
[21] G. M. Staebler, N. T. Howard, J. Candy, and C. Holland 2017 Nucl. Fusion **57** 066046,
[22] P. Rodriguez-Fernandez et al 2019 Phys. Plasmas to be published.
[23] G. V. Pereverzev, P. N. Yushmanov 2002 Report IPP 5/98 MPI fur Plasmaphysik, Garching.
[24] E. Fable et al 2013 Plasma Phys. Control. Fusion **55** 124028.
[25] K. Behringer 1987 JET-R(87)08, JET Joint Undertaking, Culham.
[26] R. Dux et al 1999 Nucl. Fusion **39** 1509.
[27] R. Dux 2007 Report IPP 9/82 MPI fur Plasmaphysik, Garching.
[28] E. Fable et al 2016 Nucl. Fusion **56** 026012.
[29] R. Dux et al 2017 Nucl. Materials Energy **12** 28–35.
[30] R. Fischer et al 2010 Fusion Sc. Tech. **58** 675.
[31] S. S. Denk et al 2018 Plasma Phys. Control. Fusion **60** 105010.
[32] A. Mlynek et al 2011 Nucl. Fusion **51** 043002.
[33] M. Willensdorfer et al, 2014 Plasma Phys. Control. Fusion **56** 025008.
[34] E. Viezzer et al 2012 Rev. Sci. Instrum. **83** 103501.
[35] R.M. McDermott et al 2014 Nucl. Fusion **54** 043009.
[36] B. Baiocchi et al 2015 Nucl. Fusion **55** 123001.
[37] F. Koechl et al 2017 Nucl. Fusion **57** 086023.
[38] S. Breton et al 2018 Nucl. Fusion **58** 096003.
[39] I. Erofeev et al 2017 Nucl. Fusion **57** 126067.
[40] N. Bonanomi et al 2018 Nucl. Fusion **58** 026028.

[41] Hong-Juan Sun et al 2010 Plasma Phys. Control. Fusion **52** 045003.
[42] Yong Liu et al 2019 Nucl. Fusion **59** 044005.